Oceanological and Hydrobiological Studies

International Journal of Oceanography and Hydrobiology

Volume 54, No. 4 December 2025
pages (303-327)

ISSN 1730-413X
eISSN 1897-3191

Aboveground biomass growth mapping and CO_2 uptake of multispecies seagrass meadow in Menjangan Besar Island, Karimunjawa Islands, using Sentinel-2 imagery

by

Aurellia Devina Putri[1],
Pramaditya Wicaksono[2,*]

DOI: **https://doi.org/10.26881/oahs-2025.1.27**
Category: **Original research papers**
Received: **May 17, 2025**
Accepted: **November 21, 2025**

[1]*Blue Carbon Research Group, Faculty of Geography, Universitas Gadjah Mada. Indonesia 55281*

[2]*Department of Geographic Information Science, Faculty of Geography, Universitas Gadjah Mada, Indonesia 55281*

* Corresponding author: *prama.wicaksono@ugm.ac.id*

Abstract

Seagrasses absorb CO_2 for photosynthesis and convert it into new biomass. This study aims to assess the correlation between seagrass aboveground biomass (AGB) growth and percent cover, map and analyse AGB growth using Sentinel-2 imagery and estimate CO_2 uptake by multispecies seagrass meadows on Menjangan Besar Island. Correlation analysis revealed a strong relationship between AGB growth and percent cover at the community level (r = 0.64) and for *Enhalus acoroides* (r = 0.60), and a very strong relationship for *Thalassia hemprichii–Cymodocea rotundata* assemblages (r = 0.89). AGB growth mapping was conducted using random forest (RF) regression, resulting in root mean square errors (RMSE) of 60.8, 125.6, 94.2 and 94.9 gDW · m^{-2} · $year^{-1}$ for *E. acoroides*, *T. hemprichii–C. rotundata*, *E. acoroides–T. hemprichii*, and bare substrate (BS) classes, respectively. The corresponding coefficients of determination (R^2) were 0.87, 0.67, 0.70, and 0.78. The total seagrass AGB growth on Menjangan Besar Island was estimated at 672.21 MgDW · $year^{-1}$, with an average of 331.7 gDW · m^{-2} · $year^{-1}$. The estimated total CO_2 uptake by seagrass meadows was 197.85 $MgCO_2$ · $year^{-1}$, with an average of 97.6 gCO_2 · m^{-2} · $year^{-1}$.

Key words: aboveground biomass growth, multispecies seagrass meadow, CO_2 uptake, random forest, Sentinel-2

1. Introduction

Global warming refers to the increase in Earth's temperature caused by greenhouse gas emissions trapped in the atmosphere (Lee et al., 2007). Indonesia, a nation where fossil fuel combustion is deeply embedded in daily activities, has experienced a notable rise in air temperatures, with an annual average anomaly of 0.6°C reported in 2016 (Sulistyono, 2012). One significant impact of global warming in Indonesia is the heightened risk of coastal inundation in major cities, such as Jakarta and Surabaya, due to rising sea levels. This phenomenon threatens coastal ecosystems, including seagrass meadows, whose growth is adversely affected by elevated seawater temperatures and increased wave energy (Tang & Hadibarata, 2022). To safeguard coastal ecosystems, adaptation and mitigation strategies are essential, particularly those that aim to limit global temperature increases to 1.5°C (Rogelj et al., 2018). Nature-based solutions play a critical role in these efforts, with carbon biosequestration emerging as a key approach. Carbon biosequestration involves the capture and storage of atmospheric carbon dioxide (CO_2) by living organisms (Howard et al., 2018). The United Nations Environment Program (UNEP) highlights that beyond their role in carbon biosequestration, seagrass meadows provide essential ecosystem services and offer a sustainable solution for enhancing coastal resilience. Consequently, seagrass ecosystems are among the most effective nature-based solutions for combating climate change (UNEP, 2020).

Seagrass is a marine angiosperm that forms an integral part of coastal ecosystems, thriving in shallow marine environments (Fauzan & Wicaksono, 2021; Wicaksono et al., 2019). Globally, 58 seagrass species have been identified, 13 of which are found in Indonesia (Kuo, 2007). Among the regions in Indonesia with extensive seagrass meadows is the Karimunjawa Islands, designated as part of the national forest. In this area, seagrass meadows are widely distributed along the coastline, with percent cover ranging from 9% to 83.33% (Nababan et al., 2010). Seagrass ecosystems provide numerous critical ecological, social and economic benefits. Ecologically, they function as primary producers and serve as habitats and nursery grounds for various marine species, including fish, shellfish and turtles (Guinotte & Fabry, 2008). Socially, seagrass meadows support local fisheries, acting as vital fishing grounds for coastal communities and contributing to food security (Arkham et al., 2015). Economically, seagrass and macroalgae ecosystems have an estimated annual value of up to US$19000 per hectare, which is 23–33 times higher than the average economic value of marine and terrestrial ecosystems, three times higher than coral reefs and 10 times higher than tropical forests (Björk et al., 2008; Costanza et al., 1997).

Seagrass, as an autotrophic plant, produces its own food through photosynthesis (Amrullah & Roza, 2018). This process requires carbon dioxide (CO_2) to dissolve from the atmosphere into seawater, enabling seagrass to play a significant role in absorbing CO_2 emissions (Hori et al., 2019), which account for approximately 56% of all carbon emissions from human activities globally (IPCC, 2021). The ability of seagrass to absorb CO_2 can be estimated by measuring the biomass produced through photosynthesis (McRoy, 1974; UNEP, 2020). This biomass contributes to the formation of new organic material, such as living biomass, litter and standing stock, highlighting the role of seagrass as a primary producer (Kaswadji et al., 2012). However, the growth of biomass and CO_2 uptake varies across species due to internal factors, such as species-specific traits and external factors, including temperature, salinity, turbidity, substrate type and nutrient availability (Riniatsih et al., 2018; Udy & Dennison, 1997).

Although nature-based solutions involving seagrass are recognised for their potential in reducing carbon emissions, data on seagrass carbon biosequestration remains limited (Ginting, 2023). This limitation is partly due to the challenges in obtaining seagrass data, compounded by the vast seagrass areas in Indonesia, totalling approximately 1.9 million hectares, which remain unmapped (Wahyudi et al., 2020). The constraints are further exacerbated by the unique characteristics of seagrass habitats, which are located in shallow coastal waters and require field surveys that account for seasonal variations and tidal conditions. Additionally, the field data typically collected consist of point-based measurements, which are subsequently interpolated (Adi et al., 2019; Graha et al., 2016). Consequently, this approach often fails to capture the spatial heterogeneity of seagrass ecosystems.

Remote sensing provides a valuable tool for mapping seagrass meadows, as visible wavelengths can penetrate shallow waters and effectively capture object reflectance (Bukata et al., 1995). To accurately map carbon dioxide uptake, data with sufficient scale, detail, and resolution are essential to minimise generalisation errors (Bell et al., 2006; Kenworthy et al., 2006). Remote sensing imagery enables the extraction of key seagrass parameters, such as distribution, coverage, and biomass, which are critical for understanding biomass growth (Hossain et al., 2015). However, remote sensing-based assessments of carbon dioxide uptake by seagrass remain rare in

Indonesia. This approach holds significant potential, as it allows for more efficient annual estimates of carbon dioxide uptake (Wicaksono, 2017).

This research included three objectives. First, to analyse the relationship between aboveground biomass (AGB) growth and percentage seagrass cover. Second, to map and analyse the spatial distribution of AGB growth using Sentinel-2 imagery. Third, to estimate the amount of carbon dioxide taken up by multispecies seagrass meadows on Menjangan Besar Island.

2. Site description

The research was conducted on Menjangan Besar Island, part of the Karimunjawa Islands in Central Java, Indonesia. This island is situated southwest of Karimunjawa Island and Kemujan Island and east of Menjangan Kecil Island (Figure 1). Menjangan Besar Island is included in Karimunjawa National Park, which covers an area of 1116.25 km^2 (Wicaksono et al., 2012). The seagrass percent cover and species diversity at Menjangan Besar Island are higher compared to other islands in the Karimunjawa Archipelago, making it a suitable location for this research. The seagrasses in the Karimunjawa Islands consist of nine species: *Enhalus acoroides* (*Ea*), *Halophila ovalis* (*Ho*), *Thalassia hemprichii* (*Th*), *Cymodocea rotundata* (*Cr*), *Oceana serrulata* (*Os*), *Halodule pinifolia* (*Hp*), *Halodule uninervis* (*Hu*), *Syringodium isoetifolium* (*Si*), and *Thalassodendron ciliatum* (*Tc*). Of these, *Ea*, *Th* and *Cr* are the species found in the waters surrounding Menjangan Besar Island (Nababan et al., 2010).

3. Image data

This study utilised Sentinel-2A imagery with a 10-m ground sampling distance (GSD), encompassing red, green, blue and near-infrared (NIR) bands. The Sentinel-2A Level-2A product was used, which provides surface reflectance (SR) pixel values. The selected image was acquired on 2 May 2024, as the recordings from January to April were heavily affected by cloud cover in the study area. The 2 May 2024, image corresponded to a sea level of 0.4 m, closely matching the sea level conditions recorded during the field survey conducted from March 7 to 12, 2024, which ranged between 0.3 m and 0.8 m

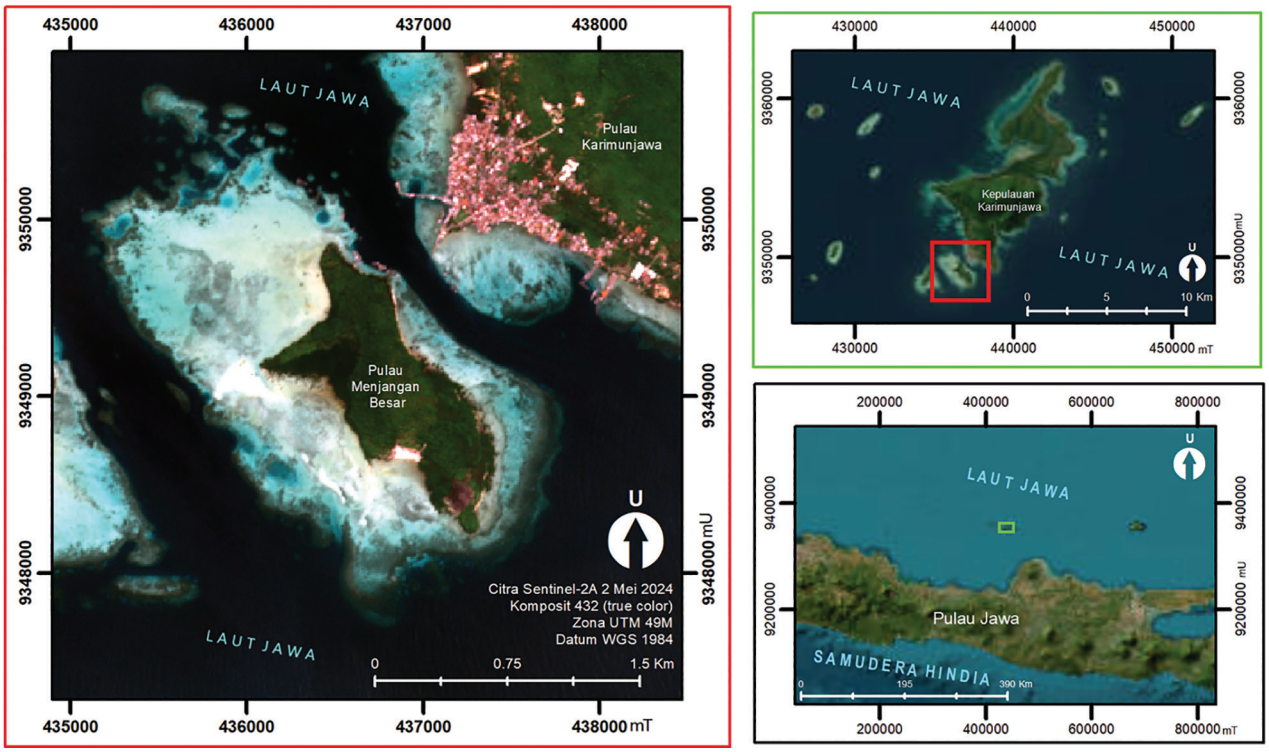

Figure 1

Menjangan Besar Island, Karimunjawa Islands (True colour composite of Sentinel-2A imagery background acquired on 2 May 2024).

(Pusat Hidro-Oseanografi TNI Angkatan Laut, 2024). Furthermore, the May acquisition date was chosen due to its alignment with the seagrass growth season, which is similar to that of March.

Seagrass growth seasons can vary throughout the year, particularly during the rainy season (January–March), the transition period from rainy to dry season (April–June), the dry season (July–September) and the transition from dry to rainy season (October–December). These seasonal differences are influenced by light availability, which subsequently affects seawater temperature (Kim et al., 2015; Patriquin et al., 2024; Wicaksono et al., 2022). During the rainy season, reduced sunlight and lower seawater temperatures create suboptimal conditions for seagrass growth. Conversely, the dry season, characterised by increased light and higher seawater temperatures, provides more favourable conditions. However, excessively high seawater temperatures can induce physiological stress in seagrass, potentially leading to mortality (Ralph et al., 2007).

4. Methods

4.1. Image corrections

Image correction involves addressing atmospheric effects, sunglint, and water column effects to improve the quality of Sentinel-2 imagery. Atmospheric correction was first conducted using ACOLITE (Atmospheric Correction for OLI Lite) (Vanhellemont & Ruddick, 2016), which is specifically designed for coastal and inland waters. The dark spectrum fitting (DSF) algorithm within ACOLITE was applied to derive SR by minimising atmospheric scattering effects, particularly in the visible and NIR regions. Sunglint correction was then performed using the method proposed by Hedley et al. (2005), which establishes a linear relationship between NIR and visible bands through linear regression based on selected pixel samples, including low, medium, and high sunglint regions from the image. The resulting sunglint-corrected bands are referred to as the deglinted image. Subsequently, water column correction was applied to the deglinted image using the Lyzenga (1978) method, also known as the depth invariant index (DII). This method assumes that variations in reflectance values for the same object are caused by differences in water depth, while the attenuation coefficient remains constant across each band (Zoffoli et al., 2014). The resulting water column-corrected imagery is referred to as the DII image.

4.2. Image masking

Image masking was performed to exclude land, optically shallow water and deep water pixels from the mapping process. The boundaries of the land area were identified using the NDVI transformation applied to the SR image, where land pixels yielded values > 0, and water pixels had values <0. The boundary between optically shallow and deep water was determined using unsupervised K-Means classification, as the K-Means algorithm effectively groups similar pixel values into clusters. The masking process resulted in the identification of the optically shallow water area, which is the primary focus of this research. Subsequently, the masked output was used as input for principal component analysis (PCA) transformation.

4.3. PCA

PCA is an image rotation technique designed to handle datasets with multiple bands or dimensions (Danoedoro, 2012). In this study, blue, red, green, and NIR spectral bands were used as input for PCA transformation. PCA reduces redundancy and repetition in the original spectral bands by transforming them into uncorrelated components, thereby enhancing the distinctiveness of the information within each band (Lazuardi et al., 2021). The output of the PCA transformation consists of new spectral bands, referred to as principal components (PCs). These PC bands were utilised as inputs for random forest regression (RFR) scenarios for benthic habitat and seagrass species classification, which are hereafter termed PC SR bands. Additionally, the PC SR bands were inverted to obtain new noise-removed SR bands to estimate seagrass cover percentages using RFR. As a result, the PCA transformation produced two datasets: PC SR bands with non-redundant information maximised in individual bands and an inverse PCA-derived SR bands.

4.4. ISODATA classification

The iterative self-organising data analysis technique (ISODATA) is an unsupervised multispectral classification method that utilises the minimum distance to the cluster centre (Danoedoro, 2012). In this study, ISODATA was applied to classify seagrass cover, assuming uniform percent cover and species composition within each class, based on the PC bands. The classified percentage cover of seagrass was linked to AGB growth values to produce

an AGB growth map. The resulting AGB growth values were then used to estimate AGC growth (AGCG), which served as the basis for calculating carbon dioxide uptake by the seagrass meadow ecosystem. The classification parameters were set as follows: a minimum of 5 clusters and a maximum of 10, a maximum of 10 iterations, a convergence threshold of 5%, a minimum of 1 pixel per class, a maximum standard deviation of 1 for each class, a minimum inter-class distance of 5 and a maximum of 2 class pair combinations.

4.5. Random forest

Random forest (RF) is an algorithm derived from decision tree methods, which operates by constructing multiple decision trees during the training phase (Datla, 2015). In this study, the RF algorithm was employed for both classification (RFC) and regression (RFR) tasks. Classification applications included benthic habitat and seagrass species composition mapping, while regression focused on modelling seagrass percent cover and AGB growth. The parameter settings for RF varied depending on the task. For benthic habitat classification, the n_{tree} parameter ranged from 100 to 400, with m_{try} set to the square root and log of the number of predictor variables, and impurity measures based on the Gini index and entropy. These settings were applied to several types of imagery, including SR, PC SR, deglint and DII. Species composition classification used similar m_{try} and impurity function configurations but increased the n_{tree} range to 100–500. In contrast, regression models for seagrass percent cover and AGB growth utilised n_{tree} values of 100 and 200, m_{try} set to square root and log and nodesize values ranging from 2 to 5. Model performance was evaluated using specific accuracy metrics. Classification accuracy was assessed based on the highest overall accuracy using confusion matrix analysis, while regression performance was determined based on the lowest root mean square error (RMSE), the highest R^2 value and a 1:1 plot to see the distribution of the samples.

4.6. Benthic habitat mapping

4.6.1. Field survey

A benthic habitat field survey was conducted using the 1 m × 1 m photo quadrat method to obtain data on percent cover of benthic habitats, including seagrass. This method is particularly suitable for capturing the complex and patchy patterns of seagrass meadows and is assumed to provide reliable training data for image classification, even at spatial resolutions as coarse as 30 m (Wicaksono et al., 2019). Field sampling using the photo quadrat was performed along predetermined transect lines, selected based on variations in benthic habitat types and percent cover.

4.6.2. Benthic photo interpretation

Photo interpretation was performed using Coral Point Count with Excel extension (CPCe) software (Kohler & Gill, 2006). A grid-based approach was employed, placing 25 evenly distributed points on each photo. Each point was then interpreted based on the visual characteristics of the benthic habitat captured in the photo. The use of a grid ensures consistent placement of interpretation points across all photos, facilitating uniform analysis and reducing potential bias. Two classification schemes were applied: a major scheme and a minor scheme. The major scheme categorised the data into corals (Co), seagrasses (Sg), macroalgae (Ma) and bare substrates (BS). Meanwhile, the minor scheme provided a more detailed classification, including seagrass species (*Cr*, *Os*, *Ea*, *Ho*, *Hu*, *Tc*, *Th* and *Si*), BS types (carbonate sand [CSd], rubble [Rb], and sand with microbenthos [Smb]), macroalgae (brown algae [Ba], green algae [Ga], and red algae [Ra]), corals (coral [Co] and dead coral [DCA]), as well as non-biological elements such as tape, wand, and shadow.

4.7. Classification scheme for benthic habitat mapping

The benthic habitat classification scheme utilised in this study categorises habitats into four major classes: seagrass (Sg), coral (C), macroalgae (M), and BS. This scheme forms the basis for generating a benthic habitat composition map, as described by Wicaksono et al. (2023). The specific rules applied to this classification scheme are detailed in Table 1.

4.8. Seagrass AGB growth mapping

4.8.1. Field survey

Field surveys to collect data on seagrass AGB growth were conducted based on mapping units derived from aforementioned the ISODATA classification of Sentinel-2 imagery. These mapping units are assumed to represent variations in seagrass species composition and percent cover. Consequently, a stratified sampling method was employed. The field

Table 1

Rules for developing benthic habitat classification scheme for mapping seagrass AGB growth mapping.

Category	Rules
Dominant	The percent cover of a class is >80% or <80%, while other classes are <20%.
Irrelevant	The percent cover of a class is <20% so the class is not included in the classification.
Mix	The difference in percent cover between classes is <20%.
Sub-class	The difference in percent cover between classes is >20% and the subclass name is added with a '+' sign.

AGB, aboveground biomass.

data collected included the percent cover of each species and AGB growth, both measured within 1 m × 1 m plots.

AGB growth measurements were obtained using the plastochrone interval method, as described by Short and Duarte (2001). This method involves marking the base of seagrass leaves with a needle and monitoring growth over 5 days. After this period, samples were destructively harvested by cutting the roots and rhizomes below the marked area. The difference in AGB before and after harvesting was used to calculate growth. Additionally, shoot density was recorded for each 1 m × 1 m plot, with the number of shoots counted to provide further insights into seagrass biomass dynamics.

4.8.2. Classification scheme of seagrass species composition mapping

The classification of seagrass species composition used refers to the classification based on life-form as in Table 2. The classification results of the three different seagrass species classes were used to divide the AGB growth model and validation samples based on image pixels. Thus, each seagrass species had different model and validation samples.

4.8.3. Seagrass AGB growth and percent cover analysis

The analysis of AGB growth samples from 1 m × 1 m plots, collected using a stratified sampling method was conducted using CPCe. The analysis involved randomly placing 24 points on each photograph for systematic analysis. This difference in interpretation of the AGB growth photo samples differs from the interpretation of the benthic habitat photo samples due to the highly variable distribution of seagrasses. By covering a more representative range of conditions, random sampling provides a more accurate estimation of AGB growth values. However, the classification scheme used is the same as the classification scheme for interpreting benthic habitat photos (Table 2). The percent cover information for each species is then used to estimate model and estimate the AGB growth of seagrass at community and at species level.

4.8.4. Analysis and calculation of seagrass AGB growth

AGB growth is determined based on laboratory measurements of dry weight (gDW) using the gravimetric method. This method operates on the principle that organic material in biomass decomposes into carbon dioxide and water when subjected to high temperatures, leaving a residue in the form of organic ash (Fadilah et al., 2017). The determination of organic carbon content (OCC) involves three stages of heating the biomass until a constant weight is achieved: (1) drying in an oven at 105°C for 3 hr, (2) heating in a furnace at 350°C for 2 hr, and (3) further heating in a furnace at 600°C for 8 hr.

The resulting constant dry weight (DW) of the AGB is then used to calculate seagrass AGB growth, which can be expressed either per shoot or per plot. The equations for these calculations are provided in Eqs (1) and (2), based on the approach proposed by Rahmawati et al. (2019) and modified to include a 5-day growth period to account for seagrass AGB growth over 5 days.

$$\text{AGB growth per shoot} = \frac{\text{DW}}{n} \times m \quad (1)$$

$$\text{AGB growth per plot} = \text{AGB growth per shoot} \times Ds \quad (2)$$

where: DW of AGB growth, n – the number of leaves sample from leaf-marking method which is analysed in the laboratory, m – the average number of leaves in one shoot, Ds – shoot density from field sample.

4.9. Calculation of seagrass AGCG

The aboveground carbon (AGC) from seagrass biomass is calculated based on the OCC in seagrass

Table 2

Classification scheme for seagrass species composition mapping (Wicaksono & Hafizt, 2013)

Class	Species composition	Explanation
Ea	*Enhalus acoroides*	Grows and extends vertically in the water column and sometimes reaches the surface. Other life-forms may exist in this class but are not significant. (*Ea* species ≥ 70%, other species ≤ 30%)
Th-Cr	*Thalassia hemprichii*, *Cymodocea rotundata*, *Halodule uninervis*, *Syringodium isoetifolium*, *Halophila ovalis*	Grows to cover the substrate but does not extend vertically in the water column. Other life-forms may exist in this class but are not significant. (*Ea* species ≤ 70%, other species ≥ 30%)
Ea-Th	*Enhalus acoroides*, *Thalassia hemprichii*, *Cymodocea rotundata*, *Halodule uninervis*, *Syringodium isoetifolium*, *Halophila ovalis*	A mix of *Ea* and *Th*, *Cr* species with a significant percent cover ratio.

AGB growth. The OCC is determined through laboratory analysis using the gravimetric method as described by Chen and Yu (2007). AGCG values can be calculated at different scales, including per species per shoot, per species per plot, and per plot. These calculations utilise formulas adapted from Rahmawati et al. (2019), with modifications incorporating a 5-day interval to account for AGB growth over this period, as shown in Eqs (3) and (4).

$$\text{AGC growth per shoot} = \text{OCC} \times \text{AGB growth per shoot} \tag{3}$$

$$\text{AGC growth per plot} = \text{AGC growth per shoot} \times Ds \tag{4}$$

where: OCC from AGB growth, *Ds* – shoot density from field sample.

4.10. Calculation of estimated carbon dioxide uptake

The calculated AGB and AGCG values were used to estimate carbon dioxide (CO_2) uptake by seagrass meadows. The estimation was performed using the equation described in Eq. (5) (IPCC, 2006), which provides a standardised approach for converting carbon stock measurements to CO_2 absorption.

$$\text{CU} = \text{AGC growth per plot} \times \frac{44}{12} \tag{5}$$

where: $\frac{44}{12}$ – conversion factor obtained from the ratio of the molar mass of CO_2 (44 g · mol^{-1}) to the molar mass of C (12 g · mol^{-1}).

4.11. Research flowchart

The flowchart of this research is provided in Figure 2.

5. Results

5.1. Field data analysis

5.1.1. Benthic habitat data

Field surveys to collect benthic habitat data were conducted on 8, 10 and 11 March 2024, resulting in a total of 4004 benthic photos. Following geotagging using GPS and integration with Sentinel-2 imagery, 952 georeferenced benthic photos were obtained. These photos were interpreted using CPCe and served as the basis for training area and accuracy assessment of mapping benthic habitat, seagrass species composition, seagrass percent seagrass cover and seagrass AGB growth.

5.1.2. Seagrass AGB growth

The field survey conducted from 7 to 12 March 2024, to measure seagrass AGB growth resulted in 20 samples, with 10 collected from the eastern region and 10 from the western region of Menjangan Besar Island. The dominant seagrass species identified were *Ea*, *Th* and *Cr*. Notably, *Ea* was predominantly found in the eastern region, while *Th* and *Cr* were more common in the western region. *Ea* occurred in homogeneous patches, whereas *Th* and *Cr* were distributed heterogeneously across the sampled quadrat plots.

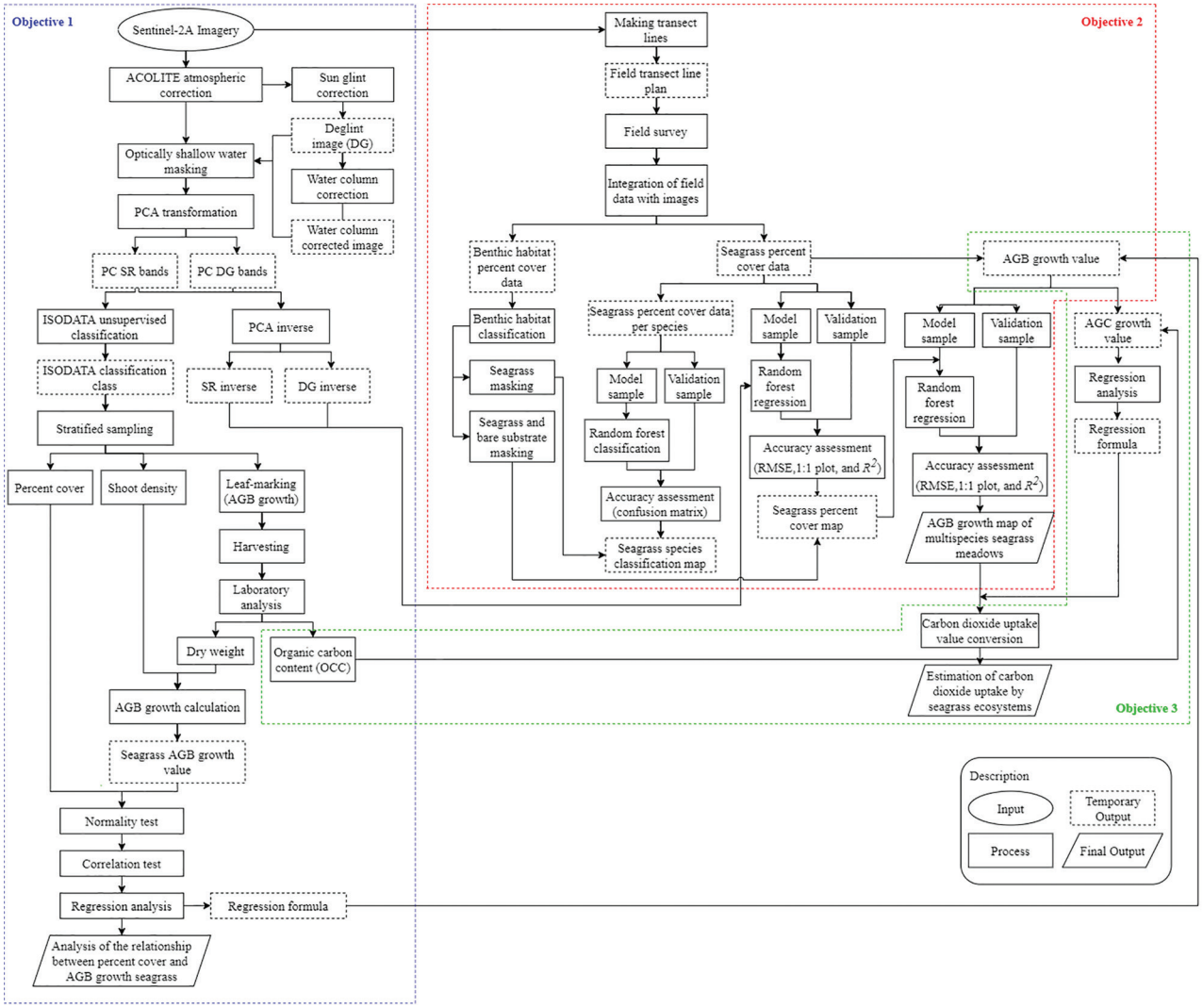

Figure 2

Research flowchart. AGB, aboveground biomass; OCC, organic carbon content; PCA, principal component analysis; RMSE, root mean square error; SR, surface reflectance.

The AGB growth assessment involved measuring leaf elongation from the initial day to the fifth day of sampling. However, adverse weather conditions, including a storm on the fourth day, caused some needles used to mark leaf growth to be dislodged, resulting in partial data loss. Consequently, AGB harvesting was limited to samples where the needles remained intact. The harvested biomass of each species was weighed individually. While AGB growth samples of *Ea* and *Th* were successfully analysed in the laboratory, *Cr* samples could not be analysed due to insufficient mass, likely attributed to its smaller biomass size and limited sample availability. To address this limitation, the AGB growth of *Cr* was assumed to be equivalent to that of *Th*, given their similar biomass structures and co-occurrence within the multispecies seagrass meadow. This assumption provides a practical approach for estimating the AGB growth of *Cr* in the absence of direct measurements.

5.2. Benthic habitat mapping

There are 952 reference datasets for benthic habitat mapping, which were divided equally into training area and accuracy assessment samples using a 50:50 split. This division scheme was selected due to the large sample size, ensuring a balanced and unbiased evaluation of classification performance. To further minimise bias, the training area and accuracy assessment samples were randomly assigned based

on transects, with stratification performed within each class according to percent cover. This approach ensured that the distribution of training area and accuracy assessment samples across classes remained consistent. The number of training area and accuracy assessment samples for each class is detailed in Table 3. In the dominated by BS class, the number of model samples slightly exceeded the validation samples due to interpreter error in determining a BS percent cover of 100% in some photos.

Benthic habitat classification using the RF method was conducted by experimenting with various combinations of n_{tree}, m_{try} and impurity functions on SR, PC SR, deglinted and DII images. The results indicate that RF classification of benthic habitats achieves the highest OA when applied to SR images with parameter settings n_{tree} set to 300, m_{try} set to log and impurity function set to Gini index. The OA for this configuration is 67.9%, which satisfies the requirements for benthic habitat mapping as specified by SNI 7716:2011 (≥60%) (Putra et al., 2023; Sari et al., 2020). The spatial distribution of benthic habitats is shown in the map in Figure 3.

Based on Figure 3, the total mapped benthic habitat area spans 3.32 km^2 and is categorised into six classes: 'Bare substrate dominated', 'Coral dominated', 'Mix of coral and bare substrate', 'Mix of coral and macroalgae', 'Mix of seagrass and bare substrate' and 'Coral + macroalgae'.

The 'Bare substrate dominated' class covers the largest area, approximately 1522 km^2 (45.8%), followed by the 'Mix of coral and bare substrate' class with 0.698 km^2 (21.0%). The 'Mix of coral and bare substrate' 'Coral dominated' class occupies 0.563 km^2 (17%), while the 'Mix of coral and macroalgae' class accounts for 0.003 km^2 (0.1%). The 'Mix of seagrass and bare substrate' class spans 0.518 km^2 (15.6%) and the 'Coral + macroalgae' class covers 0.010 km^2 (0.3%).

The distribution of benthic habitat types is dominated by the 'Bare substrate dominated' class, which is consistent with its extensive area relative to other classes. This class is found throughout most of the optically shallow waters, extending from the coastline to the regions adjacent to the 'Coral dominated' class. The 'Coral dominated' class is distributed along the outer edge of the optically shallow waters.

The 'Mix of coral and BS' class is commonly located near the coral and 'Bare substrate dominated' classes, particularly in the outer regions surrounding the 'Coral dominated' areas. The 'Mix of coral and macroalgae' class occurs between areas of 'Coral dominated', primarily in the western and southern parts of Menjangan Besar Island.

The 'Mix of seagrass and bare substrate' class exhibits a clustered pattern, primarily near the shoreline and extending towards the main reef flat of the optically shallow waters. This class is also associated with the 'Coral dominated' and 'Mix of coral and bare substrate' classes in the northeastern part of the island, where the distance between the coastline and the optically shallow sea boundary is minimal. Seagrass in this region is classified under the mixed category due to its medium to low percent cover, often interspersed with other benthic habitats, particularly BS. Lastly, the 'Coral + macroalgae' class is characterised by a scattered distribution pattern, mainly in the western and southern regions of the island.

In addition to OA, the user's accuracy (UA) and producer's accuracy (PA) are critical for evaluating the performance of individual benthic habitat classes. Table 4 presents these accuracy metrics, derived from an error matrix based on 436 samples. This number differs from the 462 samples initially recorded due to the masking of optically shallow water boundaries, which excluded samples outside the classification area. Within Table 4, the 'Mix of coral and macroalgae' class exhibits both UA and PA values of 0. This outcome reflects the small sample size for this class, with all samples misclassified during the process.

Table 3

Number of training area and accuracy assessment samples for each benthic habitat class.

Benthic habitat class	Training area	Accuracy assessment samples
'Bare substrate dominated'	219	194
'Coral dominated'	109	108
'Mix of coral and bare substrate'	67	66
'Mix of coral and macroalgae'	6	6
'Mix of seagrass and bare substrate'	79	78
'Coral + macroalgae'	10	10
Total	490	462

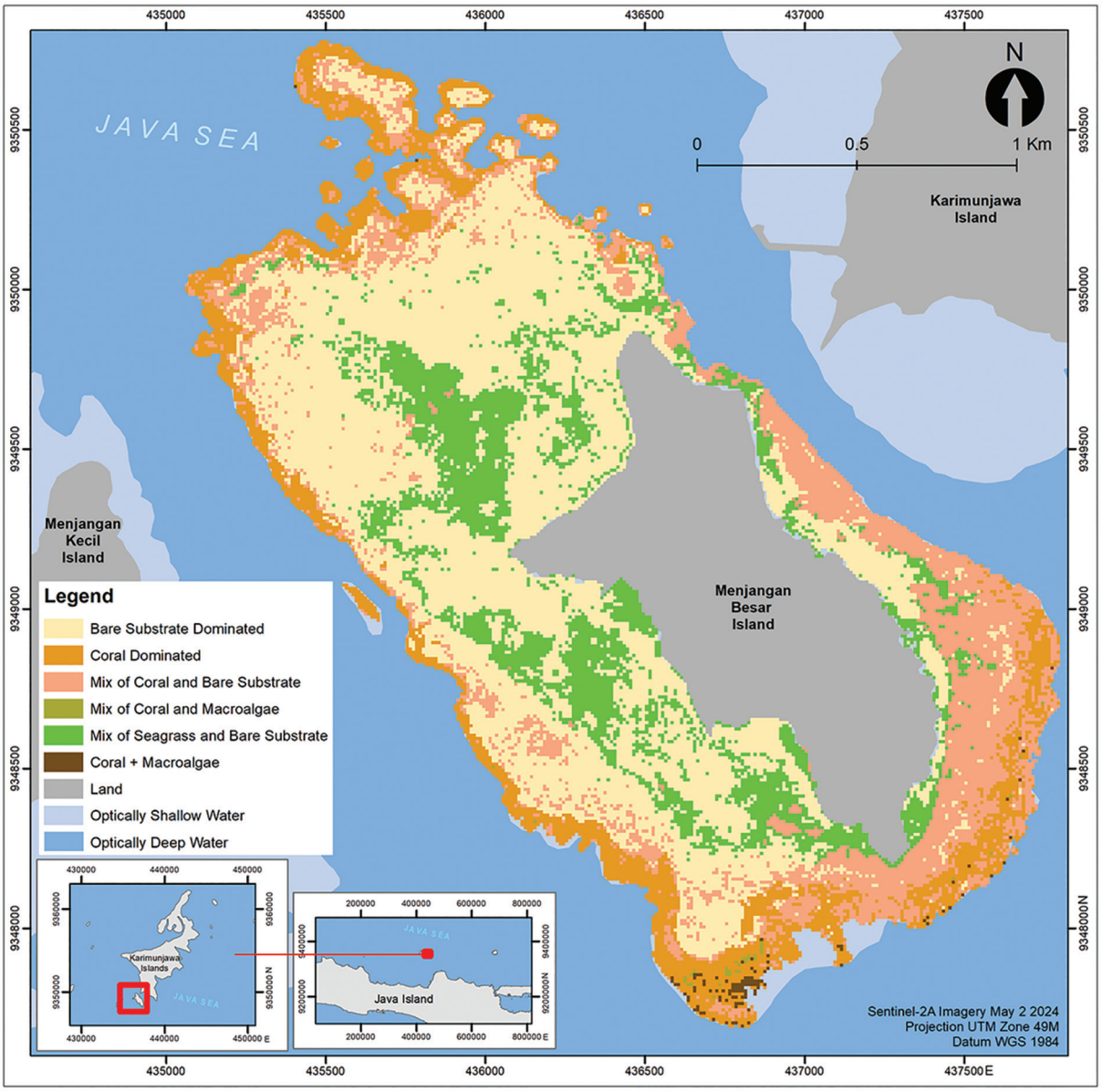

Figure 3

Benthic habitat classification result of Menjangan Besar Island (SR image: OA: 67.9%, n_{tree}: 300, m_{try}: log and impurity function: Gini index). SR, surface reflectance.

5.3. Seagrass percent cover mapping

The distribution of training area and accuracy assessment samples followed a 70:30 ratio, resulting in 117 and 48 samples respectively. Seagrass percent cover mapping was conducted on area classified as a 'Mix of seagrass and bare substrate' as well as 'Bare substrate dominated' class. 'Bare substrate dominated' class was included under the assumption that seagrass still persists in small quantities, even within areas of 'Bare substrate dominated'. Based on the experimental results, the smallest RMSE was obtained from the SR image with parameter settings of n_{tree} 200, m_{try} square root and node size 4. This configuration yielded an RMSE of 12.5%, with an r value of 0.62 and an R^2 of 0.38.

A map of seagrass percent cover is shown in Figure 4, indicating that seagrass cover ranges from 0% to 60%. The dominant cover falls within the 10%–20% and 20%–30% ranges, while the 40%–50% and 50%–60% cover ranges are less frequently observed. In general, seagrass with 10%–20% cover is concentrated near the coastline, followed by seagrass with 20%–30%

Table 4

Error matrix of benthic habitat classification using SR image, n_{tree} 300, m_{try} log and impurity function Gini index.

Classified class		Reference class							
		BSD	CD	MCBS	MCMa	MSBS	C + M	Total	UA (%)
	BSD	149	1	21	0	31	0	202	73.8
	CD	2	71	13	5	0	4	95	74.7
	MCBS	17	12	30	0	2	2	63	47.6
	MCMa	0	0	0	0	0	2	2	0
	MSBS	25	0	1	0	45	0	71	63.4
	C + M	0	1	0	1	0	1	3	33.39
	Total	193	85	65	6	78	9	436	
	PA (%)	77.2	83.5	46.2	0	57.7	11.1		OA = 67.9%

BSD, bare substrate dominated; C + M, coral + macroalgae; CD, coral dominated; MCBS, mix of coral and bare substrate; MCMa, mix of coral and macroalgae; MSBS, mix of seagrass and bare substrate; PA, producer's accuracy; SR, surface reflectance; UA, user's accuracy.

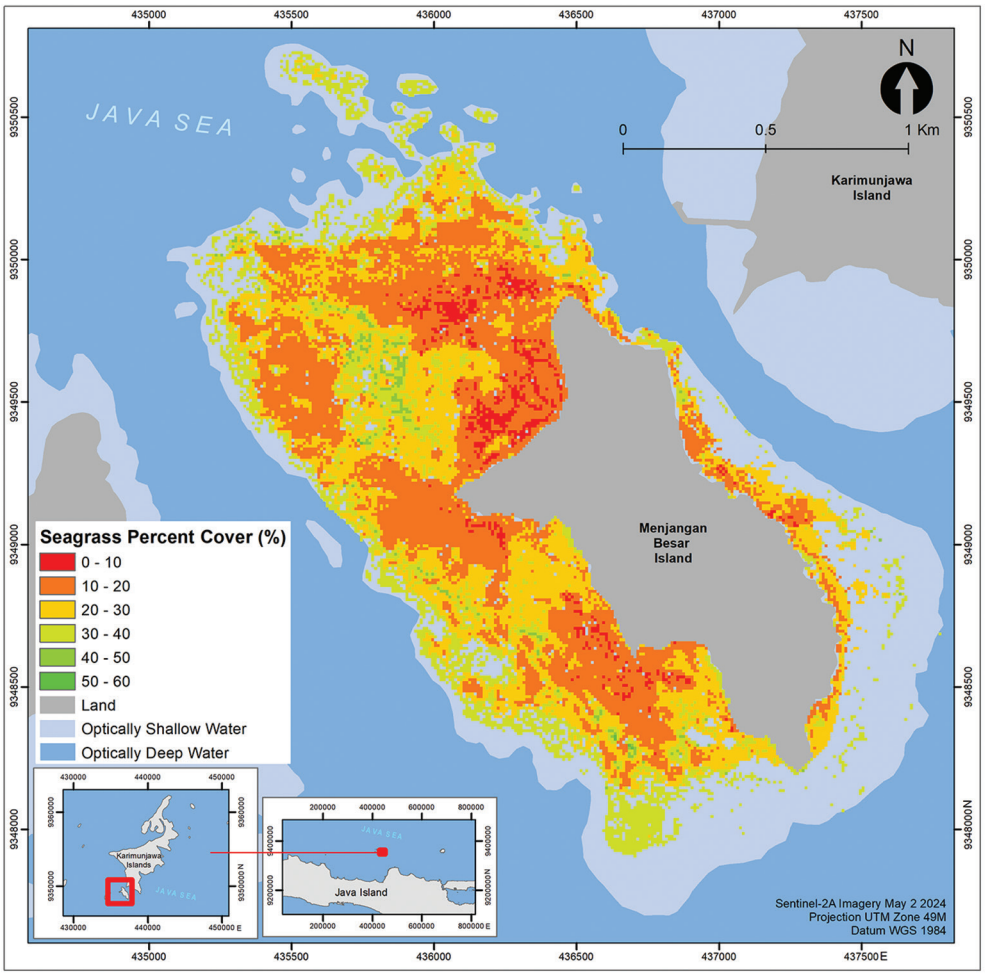

Figure 4

Map of seagrass percent cover on Menjangan Besar Island (inversed PCA-derived SR image: n_{tree} 200, m_{try} square root, nodesize 4, RMSE 12.5%, r 0.62, and R^2 0.38). PCA, principal component analysis; RMSE, root mean square error; SR, surface reflectance.

cover. Seagrass percent cover outside the 10%–30% range are more sparsely distributed but still occur in association with these dominant cover ranges.

5.4. Seagrass species composition mapping

The model sample distribution and validation for seagrass species composition mapping were conducted using a 70:30 scheme. This approach was chosen due to the limited number of seagrass species samples, totalling 110, necessitating a larger proportion of data for training the model. The sample distribution across classes was influenced by the percent cover of each seagrass species. Dominant species, such as *Ea, Th* and *Cr* were grouped into their respective classes (e.g., *Ea*, *Th-Cr*, *Ea-Th*). In contrast, mixed classes like *Ea-Th* were derived from samples where the percent cover of each species was comparable or the differences between them were minimal. Before classifying the composition of seagrass species, the four images were masked to isolate targeted benthic habitat class, specifically the mix of seagrass and BS class.

The results of the species composition classification are presented in Figure 5. The classified area covers 0.518 km^2, comprising class *Ea* with an area of 0.195 km^2 (37.6%), class *Th-Cr* with 0.268 km^2 (51.7%), and class *Ea-Th* with 0.060 km^2 (11.7%). Based on these classifications, it can be concluded that *Th-Cr* species predominantly grow in the shallow waters surrounding Menjangan Besar Island. This class is

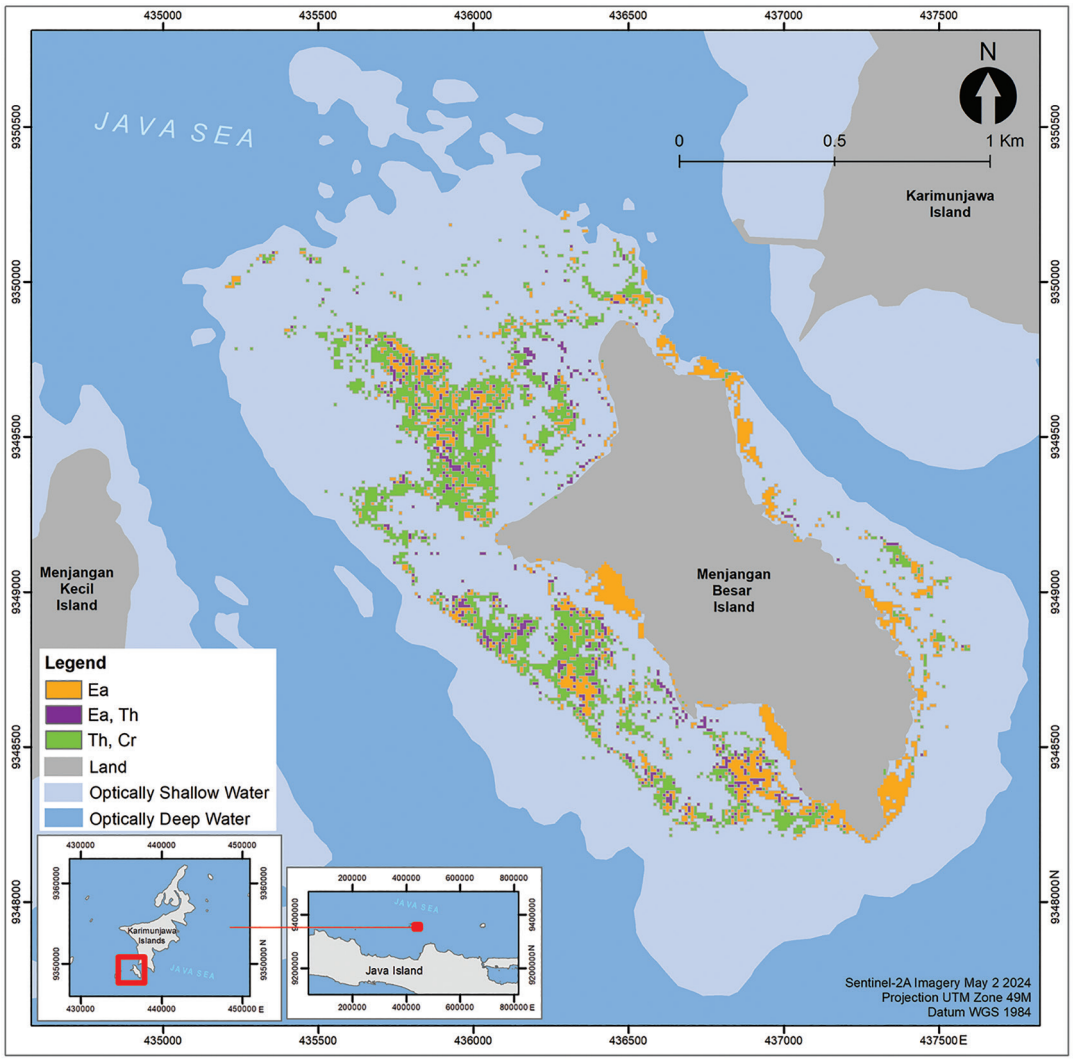

Figure 5

Map of seagrass species composition of Menjangan Besar Island (PC SR image: OA 62.5%, n_{tree} 100, m_{try} square root and impurity function entropy). PC, principal component; SR, surface reflectance.

primarily distributed in clusters along the western and southwestern parts of the island. Additionally, *Th-Cr* species are found in the northwest, often in association with other species classes.

The *Ea* species are also prevalent in shallow waters, particularly along the northeast, east, south, southwest and west coasts of the island. In contrast, the *Ea-Th* class represents the smallest area among the three classes. Unlike the other classes, the distribution of *Ea-Th* is scattered rather than clustered, often appearing in association with other classes in the northwestern, western and southwestern regions of the island. The spatial distribution patterns of these three seagrass classes align closely with field observations. Notably, *Ea* species that are not associated with other classes are commonly found near the eastern coastline, consistent with the classification results. Meanwhile, the seagrass species located in the north, northwest, west and southwest of the island typically grow in association with other species, forming multispecies seagrass meadows.

5.5. Seagrass AGB growth calculation and mapping

5.5.1. Seagrass AGB growth calculation

Seagrass AGB growth is estimated based on leaf-marking measurements. The average growth rates of seagrass leaves for *Ea, Th* and *Cr* over 5 consecutive days were 6.9 cm · leaf^{-1} · 5 days and 5.6 cm · leaf^{-1} · 5 days, respectively.

A second-order polynomial regression was applied to the community-level percent cover and AGB growth data for the *Ea* species and the combined *Th* and *Cr* (*Th-Cr*) species. The resulting R^2 and regression equations are presented in Table 5. These polynomial regression equations were used to estimate AGB growth values for seagrass based on the percent cover data from photo quadrat samples. The photo quadrat samples were categorised according to the polygons derived from seagrass species classification. Consequently, AGB growth modelling was performed for specific seagrass species classes, namely community-level AGB growth, *Ea* and *Th-Cr*. In addition, photo quadrat samples located outside these three classes, particularly those within the BS-dominated benthic habitat class, were also included in the AGB growth modelling. For each sample within the respective classes, AGB growth was calculated using the regression equations provided in Table 5.

The AGB growth values for samples of mixed *Ea-Th*, and BSs were calculated using the community AGB growth equation. This approach was chosen because the seagrass percent cover of *Ea*, *Th* and *Cr* in these samples was nearly proportional. However, the AGB growth value for samples dominated by *Ea* was calculated using the AGB growth equation specific to *Ea*, while the AGB growth values for samples dominated by *Th* and *Cr* were calculated using the equation specific to those species. The sample allocation and validation scheme for AGB growth in BSs, *Ea* and *Th-Cr* followed a 70:30 ratio, whereas for samples of *Ea-Th*, a 50:50 distribution was applied.

This difference in distribution schemes was due to the limited number of *Ea-Th* samples, which totalled only 18. To ensure a representative accuracy test and avoid overfitting in the AGB growth model for *Ea-Th*, it was necessary to increase the proportion of validation samples using a 50:50 distribution scheme. The limited availability of *Ea-Th* samples was influenced by the composition of seagrass species within the quadrat plots. Quadrat plots containing a combination of *Ea*, *Th* and *Cr* species were less common compared to those containing only *Th-Cr* or solely *Ea*, resulting in fewer samples for the *Ea-Th* category compared to the *Ea* and *Th-Cr* categories.

5.5.2. Seagrass AGB growth mapping

The results of AGB growth mapping using the RFR method are presented in Figure 6. The map was

Table 5

The R^2 value and modelling regression equation of seagrass at the community level, *Ea* and *Th-Cr* AGB growth.

Species	R^2	Regression equation
Community	0.42	$\text{AGB growth} = \left(-0.0291 \times \left(\text{PCv}^2\right)\right) + \left(13.793 \times \text{PCv}\right) + 57.885$
Ea	0.58	$\text{AGB growth}_{Ea} = \left(-0.1449 \times \left(\text{PCv}^2\right)\right) + \left(19.152 \times \text{PCv}\right) + 36.171$
Th-Cr	0.87	$\text{AGB growth}_{Th.Cr} = \left(0.191 \times \left(\text{PCv}^2\right)\right) + \left(3.3648 \times \text{PCv}\right) + 60.809$

AGB, aboveground biomass; PCv, percent cover.

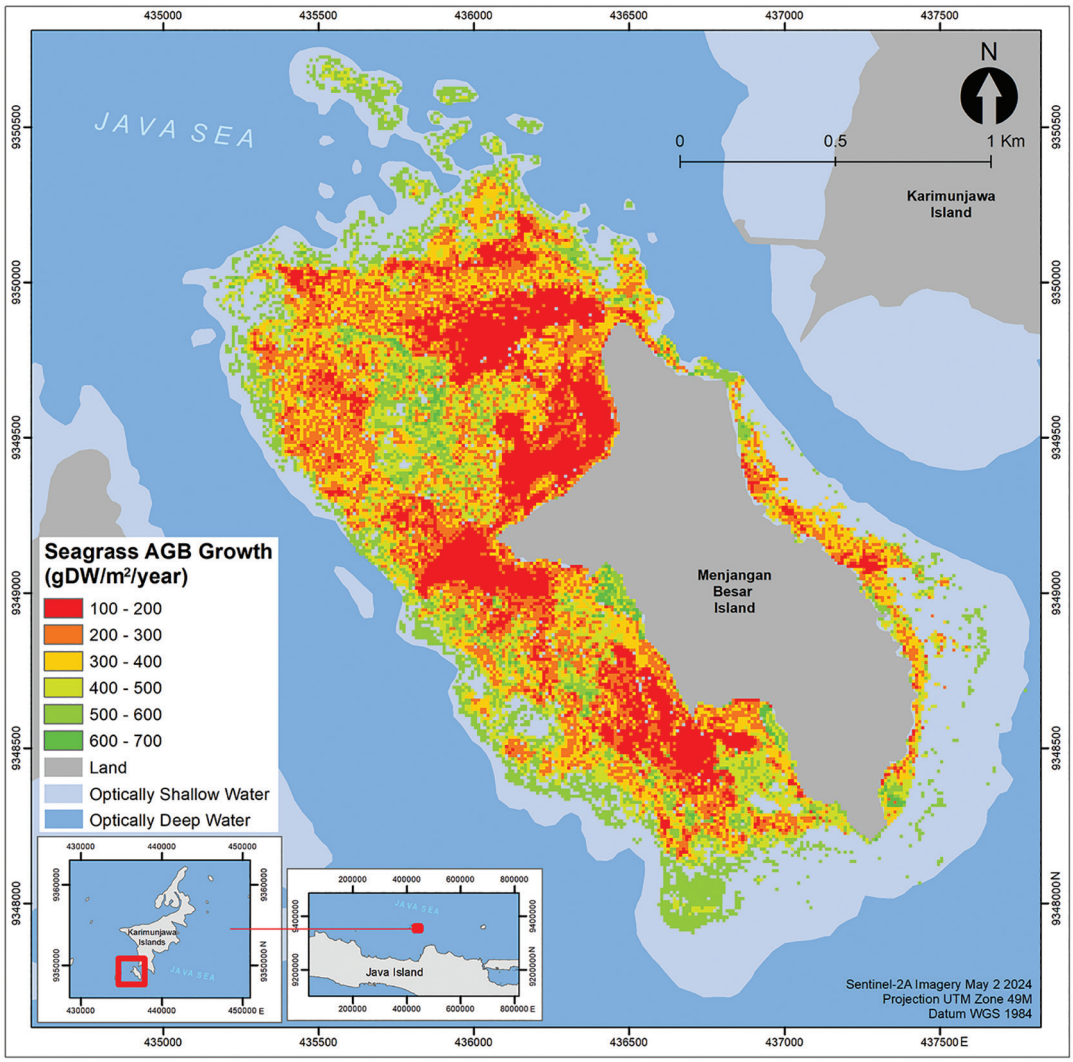

Figure 6

The AGB growth map of multispecies seagrass meadows on Menjangan Besar Island. AGB, aboveground biomass.

generated from a four-class raster mosaic representing AGB growth categories: *Ea*, *Th-Cr*, *Ea-Th*, and BS. Multispecies seagrass meadows on Menjangan Besar Island exhibit AGB growth ranging from 0 gDW · m^{-2} · $year^{-1}$ to 800 gDW · m^{-2} · $year^{-1}$. The mapped area, covering 2.03 km^2, has a total AGB growth of 672.21 MgDW · $year^{-1}$, with an average AGB growth rate of 331.7 gDW · m^{-2} · $year^{-1}$.

The dominant AGB growth values fall within the range of 200–300 gDW · m^{-2} · $year^{-1}$, which is almost evenly distributed across the optically shallow waters of Menjangan Besar Island. The second most prevalent AGB growth range, 100–200 gDW · m^{-2} · $year^{-1}$, is primarily clustered near the western and northwestern shorelines, where BSs are prevalent. These BSs exhibit lower AGB growth due to minimal seagrass cover. However, their extensive distribution in the optically shallow waters contributes to significant AGB growth within this range.

AGB growth values of 300–400 gDW · m^{-2} · $year^{-1}$ also account for a substantial area, comparable to that of the 100–200 gDW · m^{-2} · $year^{-1}$ range. This range is distributed more sporadically and is associated with other classes, without forming distinct clusters. The pixel distribution across these three value ranges indicates that the multispecies seagrass meadows on Menjangan Besar Island predominantly exhibit medium to low percent cover.

The accuracy assessment of AGB growth mapping was also conducted using R^2 values, a 1:1 scatter plot comparing the reference and estimated AGB growth data and RMSE. The R^2 values for the mapping results

of each class were 0.87, 0.67, 0.70 and 0.78, respectively. The 1:1 plots for the RFR results in each class are shown in Figure 7. Overall, the data points in the four 1:1 plots generally align with the 1:1 line, with some points closely following it, indicating similarity between the reference and estimated AGB growth values. In Figures 7A, 7C, and 7D, the distribution of points appears unbiased, suggesting minimal differences between the reference and estimated data produced by the model. However, in Figures 7B–7D, there are points that fall below the 1:1 line, indicating that the model tends to underestimate AGB growth. This underestimation is likely due to the saturation effect, where higher reference AGB growth values are not matched by corresponding increases in estimated values (Datta et al., 2024). Such saturation occurs due to the limited sensitivity of satellite sensors, which impose a threshold on reflectance values for seagrass pixels as a result of absorption by leaf pigments (Wicaksono et al., 2022).

The presence of outlier data is evident in the 1:1 plot, particularly at the points highlighted by green circles. These outliers occurred due to photo quadrate samples with unexpectedly high seagrass percent cover in the field. In the *Th-Cr* and BS class, the outlier represents the highest seagrass percent cover within that category; however, the pixel value derived from percent cover modelling was lower than that of field data with seagrass. Consequently, the estimated AGB growth value is lower than the expected reference value.

The lowest RMSE values and the optimal node size associated with the lowest RMSE varied across classes. Specifically, the RMSE values were 60.8 gDW · m^{-2} · $year^{-1}$ for *Ea*, 125.6 gDW · m^{-2} · $year^{-1}$ for *Th-Cr*, 94.2 gDW · m^{-2} · $year^{-1}$ for *Ea-Th*, and 94.9 gDW · m^{-2} · $year^{-1}$ for BSs. These results indicate that each class requires distinct RF parameter settings to achieve optimal performance (see Appendix for the complete results of the RFR tuning parameter scenario results). Therefore, conducting parameter optimisation experiments is crucial when modelling using the RFR algorithm.

5.6. Seagrass AGCG calculation

AGCG is calculated by combining the AGB growth values with the OCC growth values obtained from laboratory analysis. Laboratory results indicated that the *Ea* species had an OCC of 6.2% C_{org} · $leaf^{-1}$ · 5 $days^{-1}$, while the *Th* species exhibited a higher OCC of 11.3% C_{org} · $leaf^{-1}$ · 5 $days^{-1}$. These findings align with research by Salsabila (2024), which reported that *Th* has a higher OCC than *Ea*.

The AGCG was determined using the AGB growth values derived from leaf-marking samples. Both AGB and AGCG values were analysed through second-order polynomial and linear regression models. The second-order polynomial regression consistently yielded a higher R^2 value compared to the linear regression, particularly at the community level. Moreover, the scatter plot revealed that the data distribution aligned more closely with the trend line of the second-order polynomial regression (Table 6).

For the *Ea* and *Th-Cr* species, R^2 was 1, as the AGCG values were directly derived from the same AGB growth and OCC values, resulting in 100% of the AGCG variation being explained by the AGB growth variation. At the community level, however, the R^2 value was lower (0.88) due to the inclusion of samples from different species (*Ea* and *Th-Cr*), which exhibit varying OCC values.

The regression equation derived from the leaf-marking samples was applied to the photo quadrat samples of classes *Ea*, *Th-Cr*, *Ea-Th*, and BS to estimate the AGCG value for each sample.

The AGCG values derived from the photo quadrat samples were regressed against their corresponding AGB growth values. This regression was performed to derive an equation that could be applied to the AGB growth predictions from the RFR model for each class. As shown in Table 7, the regression results follow a second-order polynomial model for each class. The sample dataset used for this regression is consistent with the dataset used for the AGB growth RFR model, employing a 70:30 split for model training and validation, except for classes *Ea* and *Th*, which utilise a 50:50 split. The R^2 value for each class is 1.0, as the AGCG values were directly calculated from the corresponding AGB growth values.

5.7. Estimation of carbon dioxide uptake

The estimation of CO_2 uptake by seagrass meadows can be derived from the conversion of AGCG values, using the molar mass ratio of CO_2 (44/12) as outlined by IPCC (2006). This ratio is applied to modelled AGCG mapping, with the results presented in Figure 8. The total modelled CO_2 uptake by multispecies seagrass meadows on Menjangan Besar Island, which spans an area of 2.03 km^2, is estimated at 193.92 $MgCO_2$ · $year^{-1}$, with an average uptake rate of 91.9 gCO_2 · m^{-2} · $year^{-1}$. Spatial analysis reveals that CO_2 uptake values across the island range from 20 gCO_2 · m^{-2} · $year^{-1}$ to 230 gCO_2 · m^{-2} · $year^{-1}$.

The spatial distribution of CO_2 uptake exhibits a distinct pattern: lower uptake values are observed near the coastline, where BSs dominate, increasing toward the middle of shallow coastal waters and subsequently

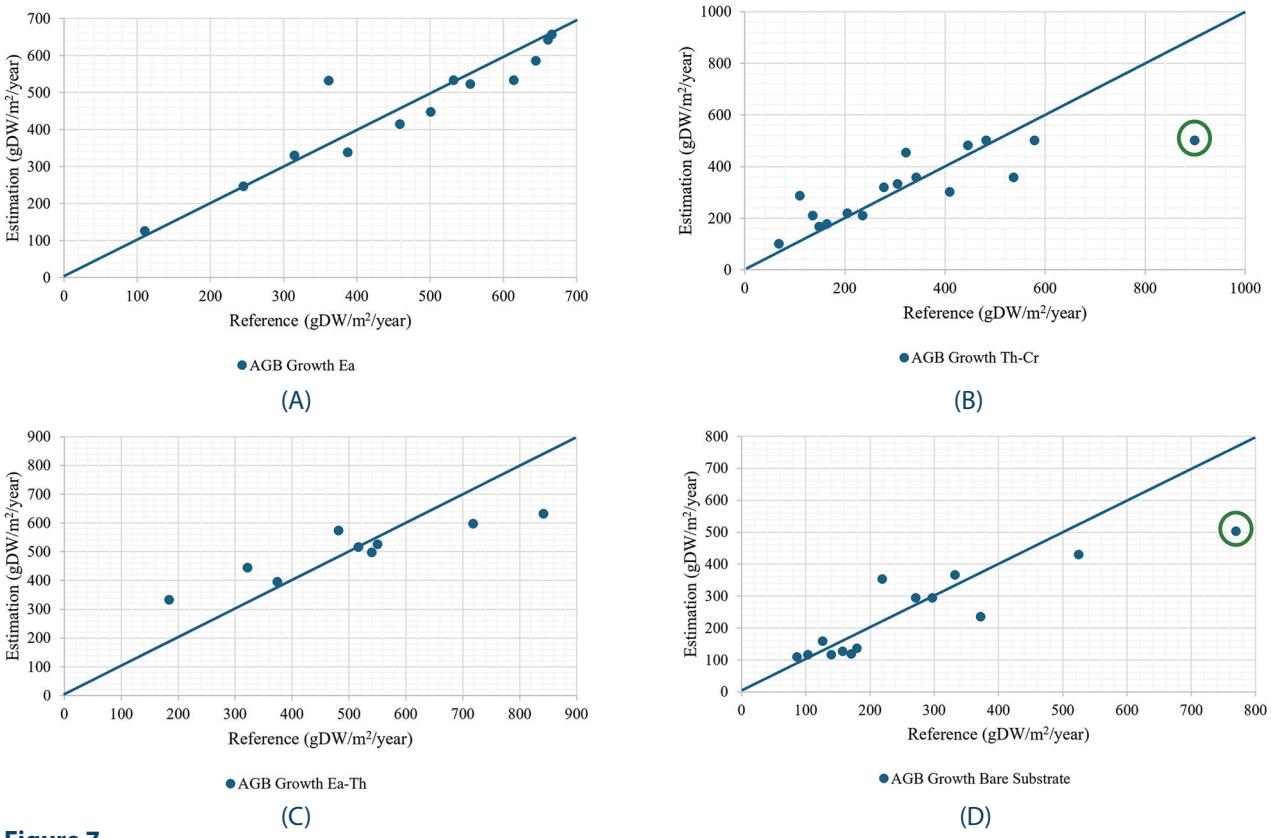

Figure 7

The 1:1 plot between reference and estimated AGB growth values for classes: **(A)** *Ea*, **(B)** *Th-Cr*, **(C)** *Ea-Th*, **(D)** BS. AGB, aboveground biomass; BS, bare substrate.

Table 6

The R^2 value and resultant regression function from: seagrass at the community level, *Ea*, and *Th-Cr* AGCG from AGBG leaf-marking samples.

Species	R^2	Regression equation
Community	0.88	$AGCG_c = ((2E{-}05) \times (AGBG_c^2)) + (0.073 \times AGBG_c) - 0.3845$
Ea	1	$AGCG_{Ea} = ((4E{-}19) \times (AGBG_{Ea}^2)) + (0.0621 \times AGBG_{Ea}) + (3E{-}13)$
Th-Cr	1	$AGCG_{Th\text{-}Cr} = ((-2E{-}19) \times (AGBG_{Th\text{-}Cr}^2)) + (0.1131 \times AGBG_{Th\text{-}Cr}) - (1E{-}13)$

AGBG, AGB growth; AGCG, AGC growth.

Table 7

The R^2 value and resultant regression function from: seagrass at the community level, *Ea*, and *Th-Cr* AGCG from photo quadrat samples of AGBG.

Class	R^2	Regression equation
Ea	1	$AGCG_{Ea} = ((2E{-}18) \times (AGBG_{Ea}^2)) + (0.0621 \times AGBG_{Ea}) + (4E{-}13)$
Th-Cr	1	$AGCG_{Th\text{-}Cr} = ((-2E{-}18) \times (AGBG_{Th\text{-}Cr}^2)) + (0.1131 \times AGBG_{Th\text{-}Cr}) + (2E{-}13)$
Ea-Th	1	$AGCG_{Ea\text{-}Th} = ((2E{-}05) \times (AGBG_{Ea\text{-}Th}^2)) + (0.073 \times AGBG_{Ea\text{-}Th}) - 0.3845$
BS	1	$AGCG_{BS} = ((2E{-}05) \times (AGBG_{BS}^2)) + (0.073 \times AGBG_{BS}) - 0.3845$

AGBG, AGB growth; AGCG, AGC growth; BS, bare substrate.

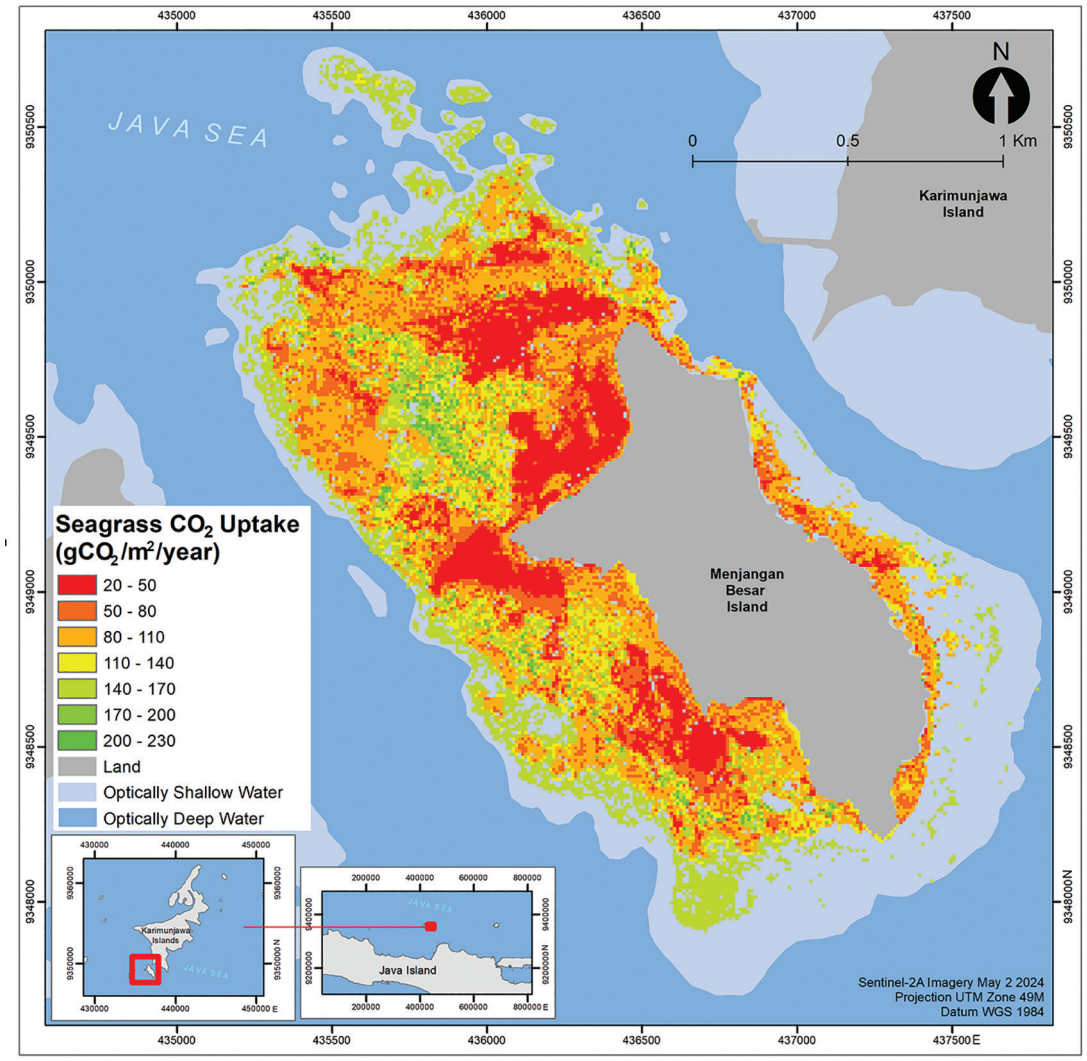

Figure 8

The CO_2 uptake estimation map of the multispecies seagrass meadow of Menjangan Besar Island.

declining in deeper waters. The most prevalent uptake values are in the ranges of 80–110, 50–80, and 20–50 $gCO_2 \cdot m^{-2} \cdot year^{-1}$, which represent the lowest tiers of uptake identified. The ranges of 80–110 $gCO_2 \cdot m^{-2} \cdot year^{-1}$ and 20–50 $gCO_2 \cdot m^{-2} \cdot year^{-1}$ are concentrated in the central parts of shallow waters, whereas the 20–50 $gCO_2 \cdot m^{-2} \cdot year^{-1}$ range also extends near the coastline, corresponding to areas with sparse seagrass cover over BSs. In contrast, the highest uptake range, 200–230 $gCO_2 \cdot m^{-2} \cdot year^{-1}$, is the least widespread and occurs sporadically, often interspersed among other uptake value ranges.

The accuracy assessment of the mapping results for estimates of CO_2 uptake by multispecies seagrass meadows on Menjangan Besar Island was conducted for each class. The RMSE values for the classes *Ea*; *Th-Cr*; *Ea-Th* and BS were 13.9, 52.1, 33.2 and 32.3 $gCO_2 \cdot m^{-2} \cdot year^{-1}$, respectively. These values indicate that the mapping error in CO_2 uptake estimates is greatest for the *Th-Cr* class. A 1:1 plot of the validation samples for each class is shown in Figure 9. The data distribution in the four 1:1 plots for CO_2 uptake estimates mirrors the distribution in the 1:1 AGB growth and AGCG plots, as carbon dioxide uptake estimates are derived from AGCG values. Consequently, the estimated R^2 values for carbon dioxide uptake in the four classes are consistent with those of AGCG, which is 0.87 for the *Ea* class, 0.76 for the *Th-Cr* class, 0.97 for the *Ea-Th* class and 0.83 for the BS class.

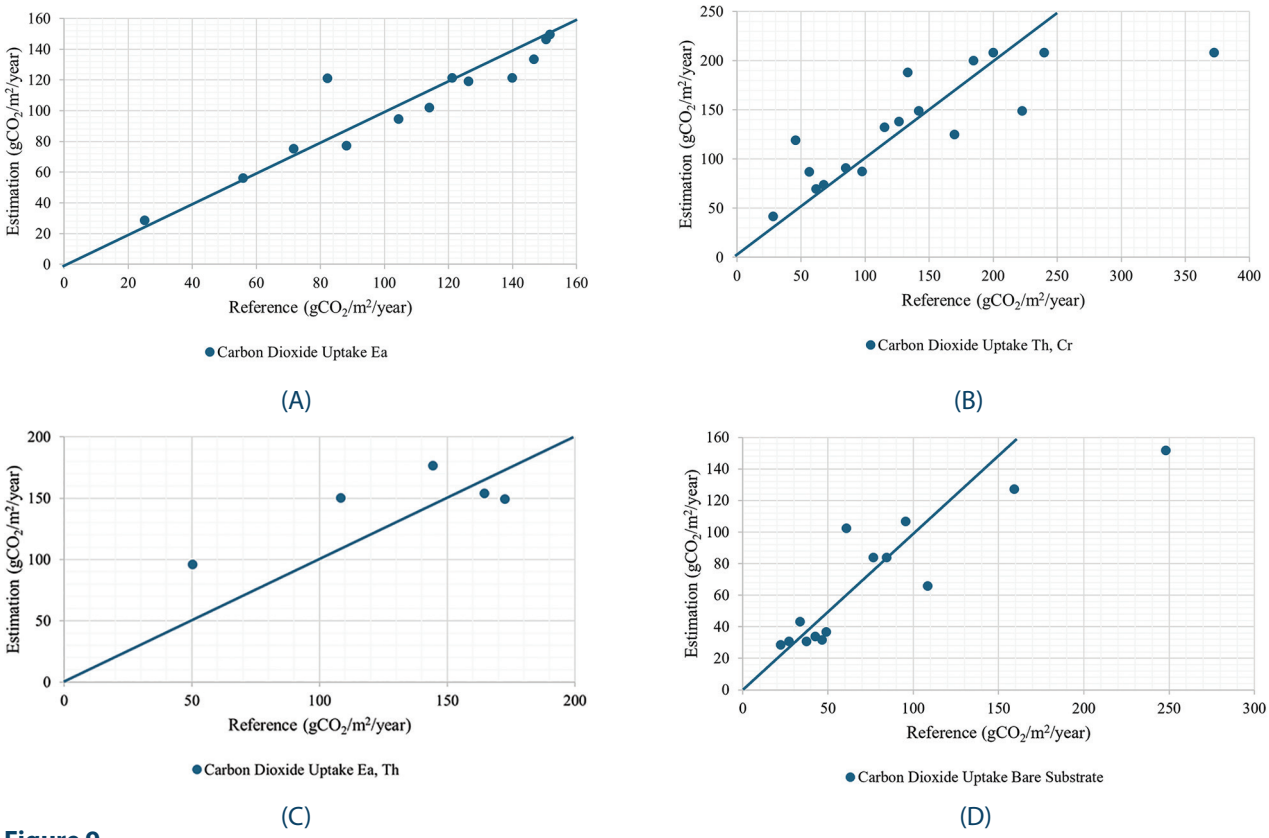

Figure 9

The 1:1 plot of field CO_2 uptake reference and estimated values for: **(A)** *Ea*, **(B)** *Th-Cr*, **(C)** *Ea-Th* and **(D)** BS. BS, bare substrate.

6. Discussion

6.1. Seagrass percent cover mapping

The seagrass percent cover on Menjangan Besar Island is categorised as low, with the dominant cover falling within the 10%–30% range. This value is lower than that of Kemujan Island, where seagrass cover is predominantly in the 60%–80% range (Wicaksono et al., 2019). Research on seagrass percent cover in other regions of Indonesia has also shown higher percent cover. For instance, studies in Labuan Bajo indicate seagrass percent cover ranging from 0% to 98.88%, with some areas reaching 100% cover (Ariasari & Wicaksono, 2019; Munir & Wicaksono, 2019). While seagrass percent cover in Indonesia generally exceeds Menjangan Besar Island, studies from other countries show similar percent cover. For example, seagrass percent cover in Moreton Bay, Australia, is predominantly between 1% and 25% (Roelfsema et al., 2009), while the average percent cover in the Indian River Lagoon, Florida, is around 20% (Morris et al., 2022). In Thailand, seagrass percent cover is 35.42% on Koh Tha Rai Island (Prathep et al., 2010) and ranges from 26% to 50% on Paklok Bay (Koedsin et al., 2016).

6.2. Seagrass AGB growth

A study by Alie (2010) conducted in the waters of Bone Batang Island, Spermonde Islands, reported an average growth rate of *Ea* leaves of 2.9 mm · leaf^{-1} · day^{-1}. Similarly, Rahman et al. (2016) observed *Ea* leaf growth rates ranging from 1.024 mm · leaf^{-1} · day^{-1} to 2.249 mm · leaf^{-1} · day^{-1}. According to Rahman et al. (2016), the primary factor influencing the growth rate of *Ea* seagrass leaves is the substrate, particularly sandy mud substrates. The growth rates reported in these studies are notably lower than the average growth rate observed on Menjangan Besar Island, where *Ea* leaves exhibited an average growth rate of 13.7 mm · leaf^{-1} · day^{-1}. Additionally, *Th* seagrass leaves on Menjangan Besar Island grew at an average rate of 11.3 mm · leaf^{-1} · day^{-1}, which is significantly higher than the growth rate of *Th* reported on Ashmore Reef, Australia, at 2.3 mm · leaf^{-1} · day^{-1} (Westlake et

al., 2022). Similar findings were reported by Haryati et al. (2022) in Tanjung Pisau, Bintan Regency, where the average growth rate of *Th* leaves was 1.77 mm · leaf^{-1} · day^{-1}. These differences in seagrass leaf growth rates can be attributed to variations in water quality parameters, substrate types and nutrient availability across study locations (Rahman et al., 2016). Thus, regional differences in environmental conditions, including water quality, substrate characteristics and nutrient levels, play a crucial role in determining seagrass growth rates.

The AGB growth value is influenced by shoot density, where an increase in the number of shoots within a plot corresponds to a higher AGB growth value for that species (Mallombasi et al., 2020). However, a high percentage of cover does not always correlate with high shoot density due to variations in species morphology (Nurdin et al., 2022). For instance, small species such as *Th* or *Cr* with a percent cover of 86.36% exhibit lower biomass compared to larger species like *Ea*, which can have a percent cover as low as 20%. Data visualisation comparing percent cover and AGB growth reveals a polynomial relationship rather than a linear one (Figure 10). The scatter plot in Figure 10A, which combines data for *Ea*, *Th* and *Cr*, indicates that while higher percent cover generally increases AGB growth, an outlier exists at 86.4% cover with an AGB growth of 1852.5 gDW · m^{-2} · year^{-1}. This anomaly is attributed to the higher shoot density of smaller species such as *Th* and *Cr*. Figure 10B, focussing on *Ea*, illustrates a decreasing trend in AGB growth at percent cover exceeding 70%, likely due to variations in leaf size. Conversely, Figure 10C demonstrates a consistently increasing trend in AGB growth with rising percent cover for *Th* and *Cr*, characterised by an upward-curving trend line.

6.3. Carbon dioxide uptake

Mapping of CO_2 uptake from seagrass AGB growth has not been conducted, whereas several studies have mapped carbon uptake from total AGB. Wahyudi et al. (2020) developed an equation to estimate carbon uptake by seagrass based on the data from 28 locations in Indonesia. According to their equation, the carbon uptake value ranges from 1.6

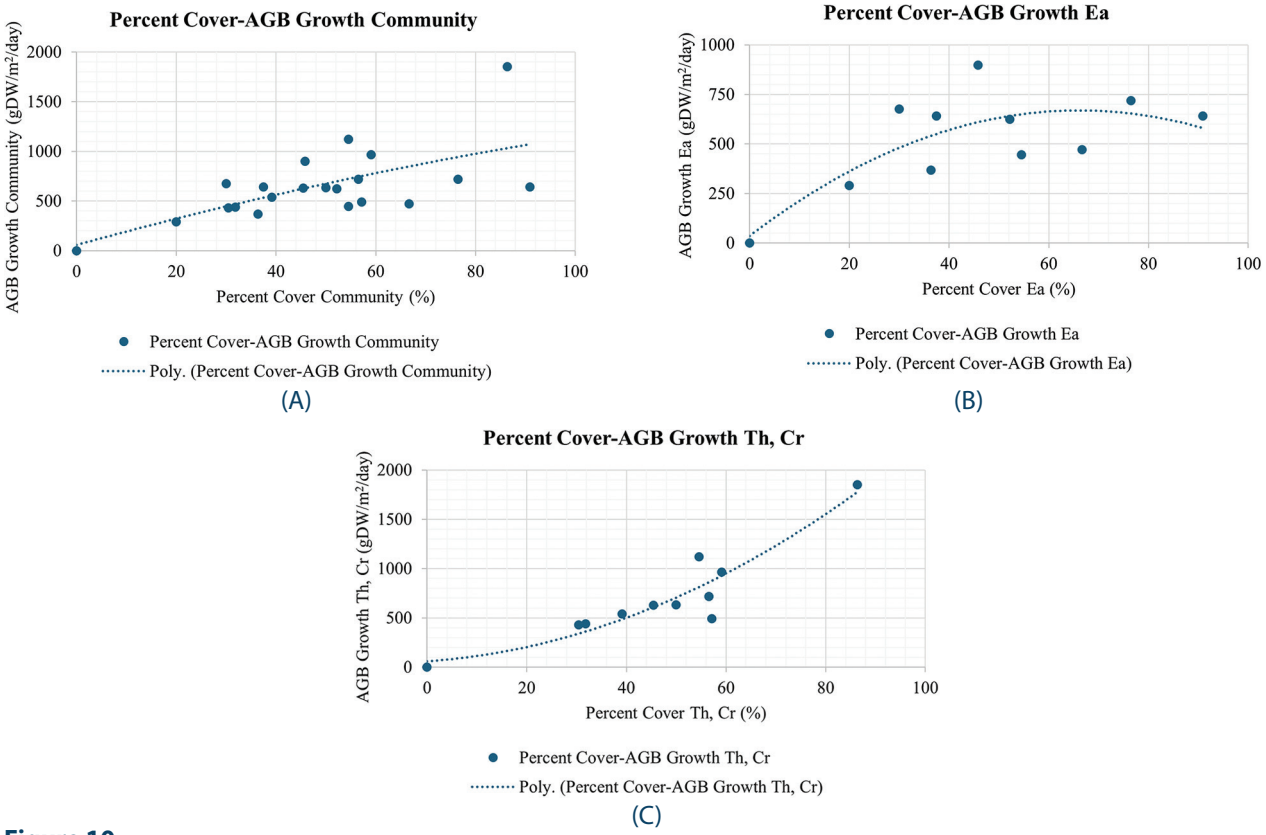

Figure 10

Relationship between seagrass percent cover and AGB growth at: **(A)** community, **(B)** species *Ea*, and **(C)** species *Th-Cr*. AGB, aboveground biomass.

MtC · year^{-1} to 7.4 MtC · year^{-1}, with the highest carbon uptake observed at Wakatobi Island, where seagrass meadows sequester 719.45 ktC · year^{-1} over an area of 11 328.05 ha. This uptake is significantly higher than the CO_2 sequestration by seagrass meadows on Menjangan Besar Island. The large carbon uptake at Wakatobi is attributed to the expansive area and high percentage of seagrass cover. In contrast, Wicaksono et al. (2022) applied Wahyudi et al. (2020) equation to estimate carbon uptake in seagrass meadows around Labuan Bajo. The mapped area encompasses 400.71 ha. The results indicated an average monthly carbon uptake of 6.7 ± 1.4 MgC · ha^{-1} · year^{-1} in 2019 and 6.6 ± 0.7 MgC · ha^{-1} · year^{-1} in 2020. The total carbon uptake for both years averaged 2648.3 ± 623.4 MgC · year^{-1} in 2019 and 2636.9 ± 281.4 MgC · year^{-1} in 2020. When compared to the mapping on Menjangan Besar Island, which covered 210.99 ha, the total carbon uptake in Labuan Bajo was greater. Additionally, numerous studies on carbon uptake by seagrass meadows outside Indonesia have been conducted. For instance, seagrass carbon uptake at Orman Reef, Australia, consisting of both monospecies and multispecies meadows, was estimated at 89.5 MgC · day^{-1} (Rasheed et al., 2008), which exceeds the estimated CO_2 uptake by multispecies seagrass meadows on Menjangan Besar Island.

Acknowledgements

We extend our gratitude to the survey team members from the Cartography and Remote Sensing program at Universitas Gadjah Mada for their assistance with seagrass AGB growth sampling, as well as to Setiawan Djody Harahap, Huwaida Nur Salsabila and Jennifer Wijaya from the Blue Carbon Research Group, Faculty of Geography, Universitas Gadjah Mada, for guiding the sampling methods and providing support with data processing both before and after the field survey.

References

Adi, W., Nugraha, A. H., Dasmasela, Y. H., Ramli, A., Sondak, C. F. A., & Sjafrie, N. D. M. (2019). Struktur Komunitas Lamun di Malang Rapat, Bintan. *Jurnal Enggano, 4*(2), 148–159. https://doi.org/10.31186/jenggano.4.2.148-159

Alie, K. (2010). Pertumbuhan dan Biomassa Lamun *Thalassia hemprichii* di Perairan Pulau Bone Batang, Kepulauan Spermonde, Sulawesi Selatan. *J. Sains MIPA, 16*(2), 105–110.

Amrullah, M. Y., & Roza, S. Y. (2018). Analisa Status dan Kondisi Padang Lamun di Kawasan Pantai-Pantai Wisata Kota Padang. *UNES Journal of Science Research, 3*(2), 110–118.

Ariasari, A., & Wicaksono, P. (2019). Random forest classification and regression for seagrass mapping using PlanetScope image in Labuan Bajo, East Nusa Tenggara. In T. D. Pham, K. D. Kanniah, K. Arai, G. J. P. Perez, Y. Setiawan, L. B. Prasetyo, & Y. Murayama (Eds.), *Sixth International Symposium on LAPAN-IPB Satellite* (p. 77). SPIE. https://doi.org/10.1117/12.2541718

Arkham, M. N., Adrianto, L., & Wardiatno, Y. (2015). Studi Keterkaitan Ekosistem Lamun dan Perikanan Skala Kecil (Studi Kasus: Desa Malang Rapat dan Berakit, Kabupaten Bintan, Kepulauan Riau). *Jurnal Sosial Ekonomi Kelautan Dan Perikanan, 10*(2), 137–148. https://doi.org/10.15578/jsekp.10.2.2015.137-148

Bell, S. S., Fonseca, M. S., & Stafford, N. B. (2006). Seagrass ecology: New contributions from a landscape perspective. In *Seagrasses: Biology, ecology and conservation* (Editor Anthony W.D. Larkum, Robert J. Orth, Carlos M. Duarte) (pp. 625–645). Springer Netherlands. https://doi.org/10.1007/978-1-4020-2983-7_26

Björk, M., Short, F., Mcleod, E., & Beer, S. (2008). *Managing seagrasses for resilience to climate change*. IUCN, Gland, Switzerland. 56pp. https://www.researchgate.net/publication/225304293

Bukata, R. P., Jerome, J. H., Kondratyev, K. Y., & Pozdnyakov, D. V. (1995). *Optical properties and remote sensing of inland and coastal waters*. CRC.

Chen, X., & Yu, J. Z. (2007). Measurement of organic mass to organic carbon ratio in ambient aerosol samples using a gravimetric technique in combination with chemical analysis. *Atmospheric Environment, 41*(39), 8857–8864. https://doi.org/10.1016/j.atmosenv.2007.08.023

Costanza, R., d'Arge, R., de Groot, R., Farber, S., Grasso, M., Hannon, B., Limburg, K., Naeem, S., O'Neill, R. V., Paruelo, J., Raskin, R. G., Sutton, P., & van den Belt, M. (1997). The value of the world's ecosystem services and natural capital. *Nature, 387*(6630), 253–260. https://doi.org/10.1038/387253a0

Danoedoro, P. (2012). Pengantar Penginderaan Jauh Digital. ANDI.

Datla, M. V. (2015). Bench marking of classification algorithms: Decision trees and random forests – A case study using R. *2015 International Conference on Trends in Automation, Communications and Computing Technology (I-TACT-15)* (pp. 1–7). IEEE, https://doi.org/10.1109/ITACT.2015.7492647

Datta, D., Dey, M., Ghosh, P. K., & Pal, A. P. (2024). Development of a spatially explicit model of blue carbon storages in tropical mudflat environment through integrated radar-optical approach and ground-based measurements. *Ecological Informatics, 80*, 102509. https://doi.org/10.1016/j.ecoinf.2024.102509

Fadilah, U., Waluyo, J., & Subchan, W. (2017). Efektivitas Cacing Tanah (Lumbricus rubellus Hoff.) dalam Degradasi Karbon Organik Sampah Sayur Pasar Tanjung Jember. *BERKALA SAINSTEK, 5*(1), 1. https://doi.org/10.19184/bst.v5i1.5367

Fauzan, M. A., & Wicaksono, P. (2021). Characterizing Derawan seagrass cover change with time-series Sentinel-2 images. *Regional Studies in Marine Science, 48*, 102048. https://doi.org/10.1016/j.rsma.2021.102048

Ginting, D. N. B. (2023). Kajian Prosedur Pemetaan Persentase Tutupan dan Biomassa Lamun dengan Menggunakan Citra Worldvie-3 di Nusa Lembongan. Universitas Gadjah Mada.

Graha, I. Y., Arthana, I. W., & Astawa Karang, I. W. G. (2016). Simpanan Karbon Padang Lamun di Kawasan Pantai Sanur, Kota Denpasar. *ECOTROPHIC: Jurnal Ilmu Lingkungan (Journal of Environmental Science), 10*(1), 46. https://doi.org/10.24843/EJES.2016.v10.i01.p08

Guinotte, J. M., & Fabry, V. J. (2008). Ocean acidification and its potential effects on marine ecosystems. *Annals of the New York Academy of Sciences, 1134*(1), 320–342. https://doi.org/10.1196/annals.1439.013

Haryati, R. N., Zulfikar, A., & Melani, W. R. (2022). Laju Pertumbuhan dan Biomassa Daun Lamun *Thalassia hemprichii* di Perairan Tanjung Pisau Desa Penaga Kabupaten Bintan. *Jurnal Akuatiklestari, 5*(2), 108–118. https://doi.org/10.31629/akuatiklestari.v5i2.4060

Hedley, J. D., Harborne, A. R., & Mumby, P. J. (2005). Technical note: Simple and robust removal of sun glint for mapping shallow-water benthos. *International Journal of Remote Sensing, 26*(10), 2107–2112. https://doi.org/10.1080/01431160500034086

Hori, M., Bayne, C. J., & Kuwae, T. (2019). Blue carbon: Characteristics of the ocean's sequestration and storage ability of carbon dioxide. *Blue carbon in shallow coastal ecosystems* (Editor Tomohiro Kuwae, Masakazu Hori) (pp. 1–31). Springer Singapore. https://doi.org/10.1007/978-981-13-1295-3_1

Hossain, M. S., Bujang, J. S., Zakaria, M. H., & Hashim, M. (2015). Application of Landsat images to seagrass areal cover change analysis for Lawas, Terengganu and Kelantan of Malaysia. *Continental Shelf Research, 110*, 124–148. https://doi.org/10.1016/j.csr.2015.10.009

Howard, J. L., Creed, J. C., Aguiar, M. V. P., & Fourqurean, J. W. (2018). CO2 released by carbonate sediment production in some coastal areas may offset the benefits of seagrass "blue carbon" storage. *Limnology and Oceanography, 63*(1), 160–172. https://doi.org/10.1002/lno.10621

IPCC. (2006). *IPCC Guidelines for National Greenhouse Gas Inventories, Prepared by the National Greenhouse Gas Inventories Programme* (Eggleston H.S., Buendia L., Miwa K., Ngara T. and Tanabe K. (eds)). Published: IGES, Japan

IPCC. (2021). Summary for policymakers. *Climate change 2021 – The physical science basis* (Editor Masson-Delmotte, V., P. Zhai, A. Pirani, S.L. Connors, C. Péan, S. Berger, N. Caud, Y. Chen, L. Goldfarb, M.I. Gomis, M. Huang, K. Leitzell, E. Lonnoy, J.B.R. Matthews, T.K.

Maycock, T. Waterfield, O. Yelekçi, R. Yu, and B. Zhou) (pp. 3–32). Cambridge University Press. https://doi.org/10.1017/9781009157896.001

Kaswadji, R. F., Bengen, D. G., & Hutomo, M. (2012). Produktivitas Komunitas Lamun di Pulau Barranglompo Makassar. *Jurnal Akuatika, 3*(2), 159–168.

Kenworthy, W. J., Wyllie-Echeverria, S., Coles, R. G., Pergent, G., & Pergent-Martini, C. (2006). Seagrass conservation biology: An interdisciplinary science for protection of the seagrass biome. *Seagrasses: Biology, ecology and conservation* (Editor Anthony W.D. Larkum, Robert J. Orth, Carlos M. Duarte) (pp. 595–623). Springer Netherlands. https://doi.org/10.1007/978-1-4020-2983-7_25

Kim, Y. K., Kim, S. H., & Lee, K.-S. (2015). Seasonal growth responses of the seagrass *Zostera marina* under severely diminished light conditions. *Estuaries and Coasts, 38*(2), 558–568. https://doi.org/10.1007/s12237-014-9833-2

Koedsin, W., Intararuang, W., Ritchie, R., & Huete, A. (2016). An integrated field and remote sensing method for mapping seagrass species, cover, and biomass in Southern Thailand. *Remote Sensing, 8*(4), 292. https://doi.org/10.3390/rs8040292

Kohler, K. E., & Gill, S. M. (2006). Coral point count with excel extensions (CPCe): A visual basic program for the determination of coral and substrate coverage using random point count methodology. *Computers and Geosciences, 32*(9), 1259–1269. https://doi.org/10.1016/j.cageo.2005.11.009

Kuo, J. (2007). New monoecious seagrass of *Halophila sulawesii* (Hydrocharitaceae) from Indonesia. *Aquatic Botany, 87*(2), 171–175. https://doi.org/10.1016/j.aquabot.2007.04.006

Lazuardi, W., Wicaksono, P., & Marfai, M. A. (2021). Remote sensing for coral reef and seagrass cover mapping to support coastal management of small islands. *IOP Conference Series: Earth and Environmental Science, 686*(1), 012031. https://doi.org/10.1088/1755-1315/686/1/012031

Lee, O., Lester, B. T., Ma, L., Lambert, J., & Jean-Baptiste, M. (2007). Conceptions of the greenhouse effect and global warming among elementary students from diverse languages and cultures. *Journal of Geoscience Education, 55*(2), 117–125. https://doi.org/10.5408/1089-9995-55.2.117

Lyzenga, D. R. (1978). Passive remote sensing techniques for mapping water depth and bottom features. *Applied Optics, 17*(3), 379–383. https://doi.org/10.1364/AO.17.000379

Mallombasi, A., Mashoreng, S., & La Nafie, Y. A. (2020). The relationship between seagrass *Thalassia hemprichii* percentage cover and their biomass. *Jurnal Ilmu Kelautan SPERMONDE, 6*(1), 7. https://doi.org/10.20956/jiks.v6i1.9922

McRoy, C. P. (1974). Seagrass productivity: Carbon uptake experiments in eelgrass, Zostera marina. *Aquaculture, 4*, 131–137. https://doi.org/10.1016/0044-8486(74)90028-3

Morris, L. J., Hall, L. M., Jacoby, C. A., Chamberlain, R. H., Hanisak, M. D., Miller, J. D., & Virnstein, R. W. (2022). Seagrass in a changing estuary, the Indian River Lagoon, Florida, United States. *Frontiers in Marine Science, 8*. 789818. https://doi.org/10.3389/fmars.2021.789818

Munir, M., & Wicaksono, P. (2019). Support vector machine for seagrass percent cover mapping using PlanetScope image in Labuan Bajo, East Nusa Tenggara. In T. D. Pham, K. D. Kanniah, K. Arai, G. J. P. Perez, Y. Setiawan, L. B. Prasetyo, & Y. Murayama (Eds.), *Sixth International Symposium on LAPAN-IPB Satellite* (p. 112). SPIE. https://doi.org/10.1117/12.2541849

Nababan, M. G., Munasik, I. Y., Kartawijaya, T., Prasetia, R., Ardiwijaya, R. L., Pardede, S. T., Sulisyati, R., & Mulyadi, S. Y. (2010). *Status Ekosistem di Taman Nasional Karimunjawa: 2010*. Wildlife Conservation Society-Indonesia Program.

Nurdin, N., Amri, K., Mashoreng, S., & Komatsu, T. (2022). Estimation of seagrass biomass by in situ measurement and remote sensing technology on small islands, Indonesia. *Ocean Science Journal, 57*(1), 118–129. https://doi.org/10.1007/s12601-022-00054-2

Patriquin, D., Scheibling, R. E., & Filbee-Dexter, K. (2024). Shifts in biodiversity and physical structure of seagrass beds across 5 decades at Carriacou, Grenadines. *PLoS ONE, 19*(8), e0306897. https://doi.org/10.1371/journal.pone.0306897

Prathep, A., Rattanachot, E., & Tuntiprapas, P. (2010). Seasonal variations in seagrass percentage cover and biomass at Koh Tha Rai, Nakhon Si Thammarat Province, Gulf of Thailand. *Songklanakarin Journal of Science and Technology, 32*(5), 497–504.

Pusat Hidro-Oseanografi TNI Angkatan Laut. (2024). *Tabel Pasang Surut Kepulauan Indonesia 2024*. Pushidros TNI AL.

Putra, I. G. P. B. A., Putra, I. D. N. N., & Putra, I. N. G. (2023). Pemetaan Sebaran Habitat Dasar Perairan Laut Dangkal Menggunakan Citra Sentinel-2A di Teluk Gilimanuk. *Journal of Marine and Aquatic Sciences, 9*(1), 18. https://doi.org/10.24843/jmas.2023.v09.i01.p03

Rahman, A. A., Nur, A. I., & Ramli, M. (2016). Studi Laju Pertumbuhan Lamun (*Enhalus acoroides*) di Perairan Pantai Desa Tanjung Tiram Kabupaten Konawe Selatan (*Enhalus acoroides*) at Tanjung Tiram Waters North Moramo Subdistrict South Konawe Regency. *Sapa Laut, 1*(1), 10–16.

Rahmawati, S., Hernawan, U. E., McMahon, K., Prayudha, B., Prayitno, H. B., Wahyudi, A. J., & Vanderklift, M. (2019). *Blue carbon in seagrass ecosystem*. UGM Press.

Ralph, P. J., Durako, M. J., Enríquez, S., Collier, C. J., & Doblin, M. A. (2007). Impact of light limitation on seagrasses. *Journal of Experimental Marine Biology and Ecology, 350*(1–2), 176–193. https://doi.org/10.1016/j.jembe.2007.06.017

Rasheed, M. A., Dew, K. R., McKenzie, L. J., Coles, R. G., Kerville, S. P., & Campbell, S. J. (2008). Productivity, carbon assimilation and intra-annual change in tropical reef platform seagrass communities of the Torres Strait, North-Eastern Australia. *Continental Shelf Research, 28*(16), 2292–2303. https://doi.org/10.1016/j.csr.2008.03.026

Riniatsih, I., Hartati, R., Endrawati, H., Mahendrajaya, R., Redjeki, S., & Widianingsih, W. (2018). The application of environmental friendly technique for seagrass transplantation. *IOP Conference Series: Earth and Environmental Science, 116*, 012103. https://doi.org/10.1088/1755-1315/116/1/012103

Roelfsema, C. M., Phinn, S. R., Udy, N., & Maxwell, P. (2009). An integrated field and remote sensing approach for mapping seagrass cover, Moreton Bay, Australia. *Journal of Spatial Science, 54*(1), 45–62. https://doi.org/10.1080/14498596.2009.9635166

Rogelj, J., Shindell, D., Jiang, K., Fifita, S., Forster, P., Ginzburg, V., Handa, C., Kheshgi, H., Kobayashi, S., Kriegler, E., Mundaca, L., Séférian, R., & Vilariño, M. V. (2018). Mitigation pathways compatible with 1.5°C in the context of sustainable development. In: *Global Warming of 1.5°C. An IPCC Special Report on the impacts of global warming of 1.5°C above pre-industrial levels and related global greenhouse gas emission pathways, in the context of strengthening the global response to the threat of climate change, sustainable development, and efforts to eradicate poverty* [Masson-Delmotte, V., P. Zhai, H.-O. Pörtner, D. Roberts, J. Skea, P.R. Shukla, A. Pirani, W. Moufouma-Okia, C. Péan, R. Pidcock, S. Connors, J.B.R. Matthews, Y. Chen, X. Zhou, M.I. Gomis, E. Lonnoy, T. Maycock, M. Tignor, and T. Waterfield (eds.)].

Salsabila, H. N. (2024). Analisis Multitemporal Aboveground Carbon Stock dan Carbon Sequestration Lamun pada Citra PlanetScope Superdove. Universitas Gadjah Mada.

Sari, C. A., Syah, A. F., Prayudha, B., & Salatalohi, A. (2020). Pemetaan Habitat Bentik Menggunakan Citra Satelit Sentinel-2A di Pulau Liki, Papua. *Jurnal Penginderaan Jauh Dan Pengolahan Data Citra Digital, 17*(1), 33–42.

Short, F. T., & Duarte, C. M. (2001). Methods for the measurement of seagrass growth and production. *Global seagrass research methods* (Editor Frederick T. Short, Robert G. Coles) (pp. 155–182). Elsevier. https://doi.org/10.1016/B978-044450891-1/50009-8

Sulistyono. (2012). Pemanasan Global (global warming) dan Hubungannya dengan Penggunaan Bahan Bakar Fosil. *Forum Teknologi, 2*(2), 47–56.

Tang, K. H. D., & Hadibarata, T. (2022). Seagrass meadows under the changing climate: A Review of the impacts of climate stressors. *Research in Ecology, 4*(1), 27–36. https://doi.org/10.30564/re.v4i1.4363

Udy, J. W., & Dennison, W. C. (1997). Growth and physiological responses of three seagrass species to elevated sediment nutrients in Moreton Bay, Australia. *Journal of Experimental Marine Biology and Ecology, 217*(2), 253–277. https://doi.org/10.1016/S0022-0981(97)00060-9

UNEP. (2020). Out of the blue: The value of seagrasses to the environment and to people (Nia). UNEP. www.un.org/Depts/Cartographic/english/htmain.htm.

Vanhellemont, Q., & Ruddick, K. (2016). ACOLITE for Sentinel-2: Aquatic applications of MSI imagery. ESA Special Publication SP-740. Presented at the ESA Living Planet Symposium Held in Prague, Czech Republic. ESA.

Wahyudi, A. J., Rahmawati, S., Irawan, A., Hadiyanto, H., Prayudha, B., Hafizt, M., Afdal, A., Adi, N. S., Rustam, A., Hernawan, U. E., Rahayu, Y. P., Iswari, M. Y., Supriyadi, I. H., Solihudin, T., Ati, R. N. A., Kepel, T. L., Kusumaningtyas, M. A., Daulat, A., Salim, H. L., … Kiswara, W. (2020). Assessing carbon stock and sequestration of the tropical seagrass meadows in Indonesia. *Ocean Science Journal, 55*(1), 85–97. https://doi.org/10.1007/s12601-020-0003-0

Westlake, E. L., Keesing, J. K., Hardiman, L., Tonks, M., & Olsen, Y. (2022). Growth, biomass and productivity of the seagrass *Thalassia hemprichii* at Ashmore Reef, Australia. *Aquatic Botany, 183*, 103557, 1–5. https://doi.org/10.1016/j.aquabot.2022.103557

Wicaksono, P. (2017). Karakterisasi Respon Spektral Spesies Lamun *Enhalus Acoroides* dan *Cymodocea Rotundata* di Pulau Karimunjawa (Characterization of Spectral Response of Seagrass Species *Enhalus acoroides* and *Cymodocea rotundata* in Karimunjawa Island). *Majalah Ilmiah Globe, 19*(1), 1–10. https://doi.org/10.24895/MIG.2017.19-1.551

Wicaksono, P., & Hafizt, M. (2013). Mapping seagrass from space: Addressing the complexity of seagrass LAI mapping. *European Journal of Remote Sensing, 46*(1), 18–39. https://doi.org/10.5721/EuJRS20134602

Wicaksono, P., Harahap, S. D., Hafizt, M., Maishella, A., & Yuwono, D. M. (2023). Seagrass ecosystem biodiversity mapping in part of Rote Island using multi-generation PlanetScope imagery. *Carbon Footprints, 2, 19.* https://doi.org/10.20517/cf.2023.9

Wicaksono, P., Lazuardi, W., & Munir, M. (2019). Integrating image at different spatial resolutions and field data for seagrass percent cover mapping. *The International Archives of the Photogrammetry, Remote Sensing and Spatial Information Sciences, XLII-4/W19*, 487–492. https://doi.org/10.5194/isprs-archives-XLII-4-W19-487-2019

Wicaksono, P., Maishella, A., Wahyudi, A. J., & Hafizt, M. (2022). Multitemporal seagrass carbon assimilation and aboveground carbon stock mapping using Sentinel-2 in Labuan Bajo 2019–2020. *Remote Sensing Applications: Society and Environment, 27*, 100803. https://doi.org/10.1016/j.rsase.2022.100803

Wicaksono, S. G., Widianingsih, W., & Hartati, S. T. (2012). Struktur Vegetasi Dan Kerapatan Jenis Lamun Di Perairan Kepulauan Karimunjawa Kabupaten Jepara. *Journal of Marine Research, 1*(2), 1–7.

Zoffoli, M. L., Frouin, R., & Kampel, M. (2014). Water column correction for coral reef studies by remote sensing. *Sensors, 14*(9), 16881–16931. https://doi.org/10.3390/s140916881

Appendix

1. Overall accuracy of benthic habitat classification experimental results using SR, PC SR, deglint and DII images

n_{tree}	m_{try}	Impurity	Overall accuracy (%)			
			SR	PC SR	Deglint	DII
100	Square root	Gini	67.66	61.47	62.39	53.44
		Entropy	66.97	60.55	63.53	54.36
	Log	Gini	67.20	60.32	61.24	55.96
		Entropy	66.51	62.16	62.16	55.96
200	Square root	Gini	66.97	61.01	63.30	54.36
		Entropy	66.28	62.16	62.84	55.05
	Log	Gini	67.43	61.70	62.39	53.67
		Entropy	66.97	62.39	60.78	55.05
300	Square root	Gini	66.74	61.93	62.84	54.36
		Entropy	67.66	61.70	61.01	55.28
	Log	Gini	67.89	61.24	61.70	54.36
		Entropy	66.97	61.01	61.70	55.50
400	Square root	Gini	67.66	61.47	62.39	54.59
		Entropy	67.20	61.70	61.70	54.59
	Log	Gini	66.97	61.70	61.93	55.05
		Entropy	66.74	62.61	61.47	54.82

DII, depth invariant index; PC, principal component; SR, surface reflectance.

2. AGB growth calculation results for *Ea* and *Th* species

No.	Species	Percent cover (%)	Shoot density (shoot · m^{-2})	Average growth rate (cm · leaf^{-1} · 5 days)	DW (gDW · shoot^{-1} · 5 days)	AGB growth (gDW · m^{-2} · year)$^{-1}$
1.	*Ea*	90.91	75	6.86	0.117	641.34
2.		54.55	52	$n = 20$		444.66
3.		52.17	73	Sum = 157.7 cm · 5 days		624.24
4.		76.47	84	Min = 2.6		718.30
5.		36.36	43	Max = 12.8		367.70
6.		45.83	105			897.88
7.		66.67	55			470.32
8.		20.00	34			290.74
9.		30.00	79			675.55
10.		37.50	75			641.34

No.	Species	Percent cover (%)	Shoot density (shoot · m^{-2})	Average growth rate (cm · leaf^{-1} · 5 days)	DW (gDW · shoot^{-1} · 5 days)	AGB growth (gDW · m^{-2} · year)$^{-1}$
11.	*Th, Cr*	30.43	167	5.63 $n = 14$ Sum = 78.8 cm · 5 days Min = 3.9 Max = 7.7	0.035	43.09
12.		50.00	245			63.21
13.		86.36	718			185.25
14.		56.52	278			71.72
15.		31.82	170			43.86
16.		57.14	190			49.02
17.		59.09	374			96.49
18.		54.55	434			111.97
19.		39.13	209			53.92
20.		45.45	244			62.95

AGB, aboveground biomass; DW, dry weight.

3. Experimental results of RF regression modelling seagrass AGB growth

Class			*Ea*			*Th-Cr*			*Ea-Th*			BS		
n_{tree}	m_{try}	Nodesize	RMSE (gDW · m^{-2} · year^{-1}	*r*	R^2	RMSE (gDW · m^{-2} · year^{-1})	*R*	R^2	RMSE (gDW · m^{-2} · year^{-1})	*r*	R^2	RMSE (gDW · m^{-2} · year^{-1})	*r*	R^2
100	Square root	2	62.58	0.93	0.86	136.84	0.76	0.58	97.41	0.76	0.58	106.80	0.82	0.67
		3	62.16	0.93	0.86	129.22	0.80	0.64	96.54	0.80	0.64	105.40	0.82	0.67
		4	62.48	0.93	0.86	130.56	0.79	0.63	104.52	0.82	0.66	100.99	0.84	0.70
		5	62.90	0.93	0.86	127.83	0.80	0.65	112.18	0.78	0.62	94.93	0.88	0.78
	Log	2	62.48	0.93	0.87	128.91	0.80	0.64	98.82	0.77	0.59	109.29	0.81	0.65
		3	62.09	0.93	0.87	134.42	0.77	0.59	102.37	0.79	0.62	106.94	0.81	0.66
		4	63.02	0.93	0.86	133.72	0.77	0.60	104.97	0.82	0.67	95.03	0.87	0.76
		5	63.21	0.93	0.86	125.85	0.82	0.66	95.92	0.87	0.76	99.89	0.85	0.73
200	Square root	2	61.04	0.93	0.87	132.94	0.78	0.60	102.63	0.74	0.55	101.43	0.84	0.71
		3	62.11	0.93	0.86	132.32	0.78	0.61	100.14	0.78	0.61	104.07	0.83	0.68
		4	61.77	0.93	0.87	128.83	0.80	0.64	94.22	0.83	0.70	97.22	0.86	0.74
		5	64.60	0.93	0.86	125.93	0.81	0.66	102.25	0.82	0.67	97.97	0.87	0.75
	Log	2	61.34	0.93	0.87	135.83	0.76	0.58	100.43	0.76	0.58	103.97	0.83	0.69
		3	60.83	0.93	0.87	130.38	0.79	0.62	102.76	0.77	0.59	101.20	0.84	0.71
		4	61.93	0.93	0.87	130.45	0.79	0.62	97.18	0.87	0.76	98.90	0.85	0.73
		5	63.24	0.93	0.86	125.55	0.82	0.67	98.60	0.87	0.75	97.31	0.88	0.77

AGB, aboveground biomass; BS, bare substrate; RF, random forest; RMSE, root mean square error.